Author Summary

Human T-cell leukemia virus type 1 (HTLV-1) is the first retrovirus that is associated with human diseases including an aggressive leukemia derived from $CD4^+$ T cells, adult T-cell leukemia (ATL), and chronic inflammatory diseases of the central nervous system, lung, or skin. However, it remains to be elucidated how HTLV-1 induces these diseases. A viral gene, *tax*, has been considered as a critical player in HTLV-1 pathogenesis, yet Tax expression is frequently lost in ATL cells. Another viral gene, *HBZ*, is constitutively expressed in both HTLV-1 infected cells and ATL cells. However, it remains unknown how HBZ functions in the HTLV-1-related diseases. We show here that the *HBZ* induced T-cell lymphoma and chronic inflammation *in vivo* similar to those in HTLV-1 infected individuals, indicating an important role of *HBZ* in HTLV-1 associated human diseases. As observed in HTLV-1 infected individuals, effector/memory and regulatory $CD4^+$ T cells were increased in the *HBZ*-transgenic mice. Further, HBZ could interact with host transcription factors, Foxp3 and NFAT, leading to dysregulation of T_{reg} function. The T_{reg} dysregulation induced by HBZ is thought to be a critical mechanism of the HTLV-1 pathogenesis. This study sheds light on the HTLV-1 associated pathogenesis and provides an important clue to prevent or treat the human diseases.

with T_{reg} functions. These results indicate that HBZ plays a critical role in neoplastic and inflammatory diseases arising from HTLV-1 infection.

Results

HBZ transgenic mice spontaneously develop inflammatory lesions in the skin and lung

Since HTLV-1 mainly infects $CD4^+$ T cells *in vivo*, we generated Tg mice expressing the *HBZ* gene under the control of the murine *CD4*-specific promoter/enhancer/silencer (Figure S1) [13]. We analyzed the *HBZ* transgenes (Figure S1) and their expression in the three lines generated. *HBZ* gene expression was specifically detected in $CD4^+$ T cells (Figure 1A). HBZ protein was also detected in these transgenic mice (Figure 1B). The level of *HBZ* gene transcripts in line 12 was the most abundant but similar to that of endogenous expression of the *HBZ* gene in ATL cell lines (Figure 1C). Therefore, unless specifically described, we used line 12 in this study. Notably, the majority of *HBZ*-Tg mice developed skin lesions by 18 weeks of age, in contrast with no disease in non-transgenic littermates (non-Tg mice) (Figure 1, D and E). Histological analyses revealed infiltration of $CD3^+CD4^+$ T cells into the dermis and epidermis, and also the alveolar septa of the lung (Figure 1, F, G and S2), whereas no obvious evidence of inflammation in other tissues, including liver, kidney, muscle, heart, stomach, spinal cord, intestines and brain. Since massive infiltration of lymphocytes in the skin and lung was observed in line 9 and 12, but not in line 2, level of HBZ expression is likely associated with these phenotypes. Thus, *HBZ*-Tg mice spontaneously developed dermatitis and alveolitis. Similar lesions have been observed in HTLV-1 carriers, especially in those harboring large numbers of infected cells [28,29].

HBZ-Tg mice develop T-cell lymphoma after a long latent period

To study the growth-promoting activity of the *HBZ* gene, we assessed the proliferation of $CD4^+$ T cells in *HBZ*-Tg mice by incorporation of bromodeoxyuridine (BrdU), and found that the proliferation was three fold-higher than in non-Tg mice, whereas the proliferation of $CD8^+$ T cells or B cells was not altered (Figure 2A, Table S1A). Transgenic expression of *HBZ* enhances the *in vivo* proliferation of mouse T cells, as ectopic expression of *HBZ* enhances the proliferation of human T cells [13,15]. It is known that HTLV-1 transforms $CD4^+$ T cells after a long latent period in a fraction of asymptomatic carriers [7]. Analogous to the development of ATL in humans, 14 of 37 (37.8%) *HBZ*-Tg mice of all three-founder lines developed T-cell lymphomas after 16 months, in contrast with 2 of 27 non-Tg mice (7.4%) ($P<0.001$ by the logrank test) (Figure 2B). In some transgenic mice, lymphoma cells infiltrated various organs including the lung, bone marrow, spleen and liver (Figure 2C). All of the lymphomas in *HBZ*-Tg mice were $CD3^+$ and $CD4^+$ by immunohistochemical analyses when examined before the mice became moribund (Figure 2D). Lymphoma cells also expressed αβT cell receptors on their surfaces (Figure S3). Monoclonal proliferation of these lymphoma cells was shown by single strand conformation polymorphism in Vγ2-Jγ1 junction region of T cell receptor γchain gene (Figure S4). Notably, the primary lymphoma cells expressed Foxp3 at various intensities in the majority of cases (Figure 2E, Table 1), exhibiting a similar FoxP3 staining pattern to that in lymph nodes in human ATL cases (Figure S5). Thus, the T-cell lymphomas in *HBZ*-Tg mice phenotypically resemble ATL, suggesting that HBZ promotes proliferation of $CD4^+$ T cells and predisposes expressing cells to transform in due course.

Increased effector/memory and regulatory $CD4^+$ T cells in *HBZ*-Tg mice

To study the cellular basis of the lymphomagenesis and inflammation in *HBZ*-Tg mice, we analyzed the phenotype and function of T cells, especially T_{reg} cells, in 3-month-old *HBZ*-Tg line 12 mice before their pathological manifestations. $CD44^{high}$ $CD62L^{low}$ effector/memory $CD4^+$ T cells increased in *HBZ*-Tg mice (Figure 3A). CD4 single positive T cells also increased in the thymus (Figure S6). Further, not only the ratio but also the absolute number of $Foxp3^+$ T cells was markedly increased in *HBZ*-Tg mice compared with non-Tg mice, while the numbers of $Foxp3^-$ T cells were equivalent (Figure 3, B and C). Increased T_{reg} cells were also observed in thymus, lymph node and peripheral blood mononuclear cells (Figure 3D and Figure S7). We also observed the increased T_{reg} cells and effector/memory T cells in the *HBZ*-Tg line 2 (Figure S8), which showed quite lower expression of HBZ than line 12 (Figure 1C). The proportion of T_{reg} cells in skin and lung was rather low compared with that in spleen (Figure 3B and S2), indicating that $Foxp3^-$ T cells are predominant in the infiltrating T cells.

This result indicates that transgenic expression of HBZ induces systemic inflammation despite an increase in $Foxp3^+$ T_{reg} cells. It has been reported that IL-2 is critical in the homeostasis of T_{reg} cells [30]. To study mechanisms by which HBZ expression increases T_{reg} cells, we analyzed IL-2 production in the $CD4^+$ T cells of *HBZ*-Tg mice after stimulation by PMA and ionomycin. IL-2 production was not augmented in either the $Foxp3^+$ or $Foxp3^-$ populations from *HBZ*-Tg mice (Figure S9), indicating that the increase in the number of T_{reg} cells was not due to enhanced IL-2 production.

Previous studies showed that Tax is a critical viral protein for the pathogenesis of HTLV-1. Therefore, we generated Tax transgenic (*tax*-Tg) mice using the same promoter/enhancer/silencer. In the *tax*-Tg mice, we did not observe increased effector/memory T cells or T_{reg} cells (Figure S10). Thus, this increase in effector/memory T cells and T_{reg} cells was specific to HBZ and

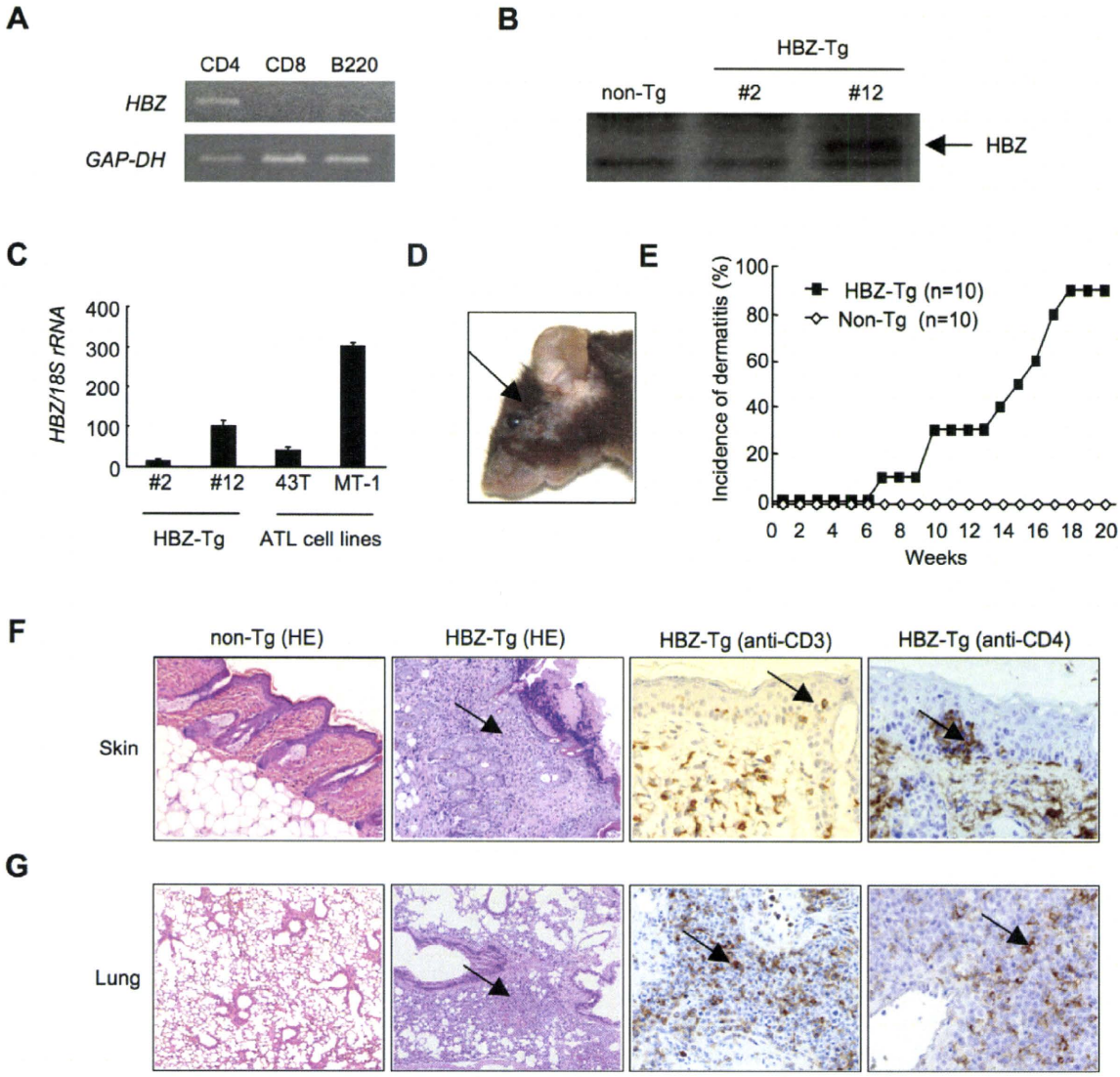

Figure 1. *HBZ*-Tg mice spontaneously develop inflammatory diseases in skin and lung. (A) Cell-type specific transcription of the transgene in line 12 was confirmed by RT-PCR in each sorted cell population. (B) The expression of HBZ protein in $CD4^+$ splenocytes was confirmed by Western blotting. (C) Transcripts of the *HBZ* gene in $CD4^+$ splenocyte of *HBZ*-Tg mice or ATL cell lines were quantified by real time PCR. ATL-43T and MT-1 are derived from ATL cells. (D) An *HBZ*-Tg mouse with typical skin symptom (Arrow indicates skin lesion). (E) The incidence of dermatitis in *HBZ*-Tg (line 12) and non-Tg mice. (F and G) Histological findings of the skin and the lung in *HBZ*-Tg mice. Lymphocytes massively infiltrated the dermis and epidermis (F) and the alveolar septum (G) (Arrows present infiltration of lymphocytes). Infiltration of $CD3^+$, $CD4^+$ T cells into these tissues was shown by immunohistochemistry compared with non-Tg mice as control.
doi:10.1371/journal.ppat.1001274.g001

not associated with similar transgenic expression of *tax* in this transgenic model system.

We next analyzed the phenotype and function of the increased $Foxp3^+$ T_{reg} cells in *HBZ*-Tg mice. $CD4^+Foxp3^+$ T cells of *HBZ*-Tg mice expressed T_{reg}-associated molecules, such as cytotoxic T-lymphocyte associated antigen-4 (CTLA-4), glucocorticoid-induced TNF receptor family-related-protein (GITR), CD103, and CD25 [31]; yet the expression levels of CTLA-4, GITR and CD25 were lower than those of $Foxp3^+$ T cells in non-Tg mice (Figure 3, B and E, Table S1B). In contrast, both $Foxp3^+$ and $Foxp3^-$ $CD4^+$ T cells of *HBZ*-Tg mice expressed CCR4 and CD103 at higher levels than those in non-Tg mice, suggesting that this might contribute to the migration and infiltration of *HBZ*-Tg $CD4^+$ T cells into the skin (Figure 1F) [32,33]. Further, it is of note that the *in vitro* suppressive function of *HBZ*-Tg T_{reg} cells was severely impaired. When $CD4^+GITR^{high}$ T cells, which were >90% $Foxp3^+$ [23], from *HBZ*-Tg or non-Tg mice were co-cultured with $CD4^+CD25^-$ T cells from wild-type mice and stimulated with Con A or anti-CD3 antibody, *HBZ*-Tg T_{reg} cells were much less suppressive (Figure 3F). These results indicate that HBZ expression increases functionally impaired T_{reg} cells.

Next, we assessed the proliferation of $CD4^+$ T cells in *HBZ*-Tg mice. BrdU incorporation of $Foxp3^+$ as well as $Foxp3^-CD4^+$ T cells from *HBZ*-Tg mice was also significantly higher than those in non-Tg mice (Figure 3G). In general, proliferation of T_{reg} cells in response to mitogenic stimulation is suppressed *in vitro*. However, $Foxp3^+$ T cells from *HBZ*-Tg mice proliferated more vigorously *in vitro* in response to anti-CD3 antibody than did non-Tg $Foxp3^+$ T cells (Figure 3H). Thus, transgenic expression of HBZ in $CD4^+$ T cells induces the expansion of $Foxp3^+$ T_{reg} cells, yet impairs their suppressive function.

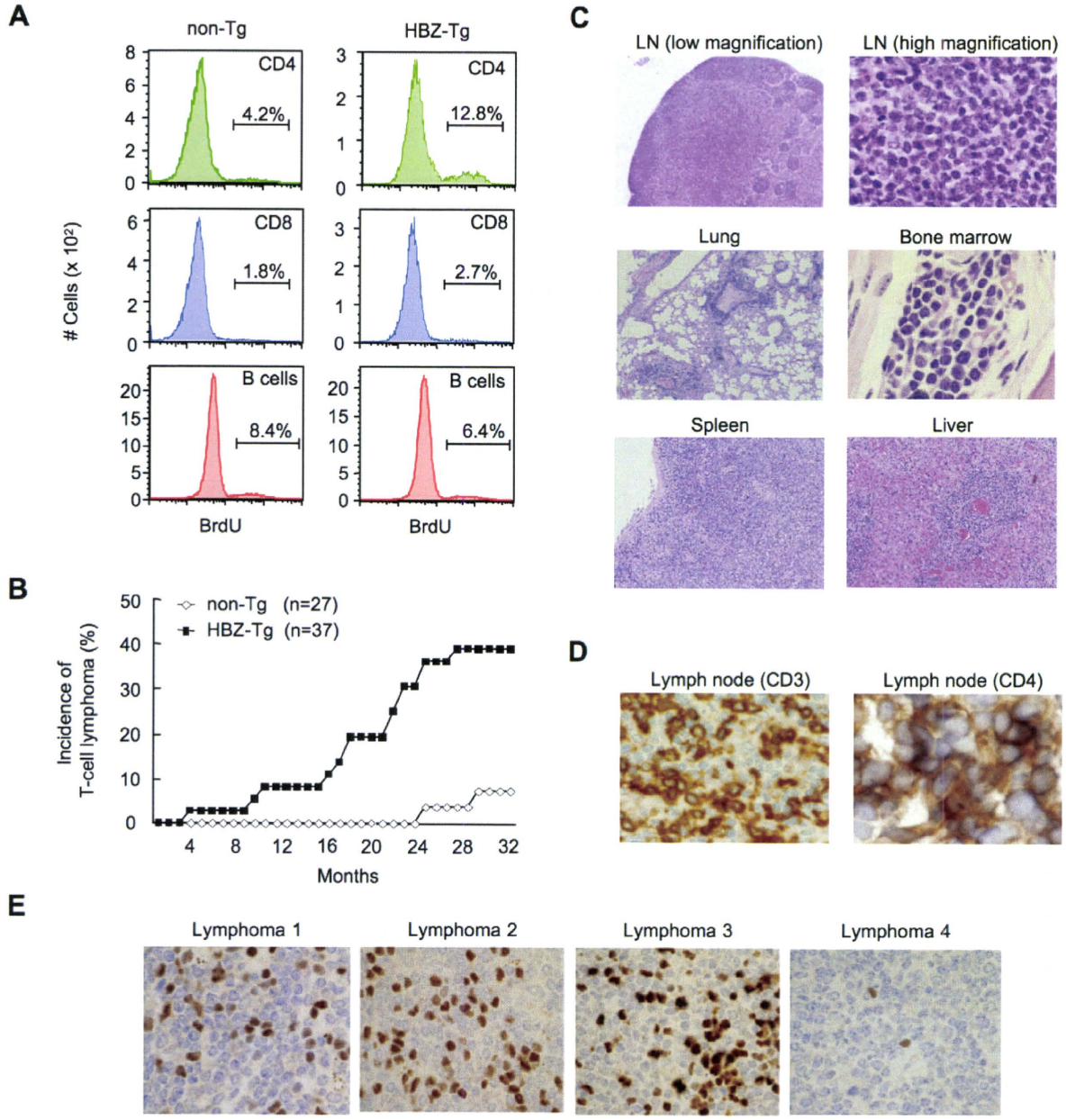

Figure 2. *HBZ*-Tg mice develop T-cell lymphoma after a long latent period. (A) BrdU was injected into mice twice a day for three days, and splenocytes were stained with antibodies to BrdU, CD4, CD8, and B220. (B) Incidence of T-cell lymphoma in *HBZ*-Tg mice was statistically significant compared with that in non-Tg mice ($P<0.001$ by the logrank test). (C) Pleomorphic lymphoma in the cervical lymph node in a representative *HBZ*-Tg mouse. Infiltrations of lymphoma cells into lung, bone marrow, spleen and liver are also shown. (D) Expression of CD3 and CD4 in lymphoma cells was shown by immunohistochemical staining. (E) Immunohistochemical staining for Foxp3 in primary lymphomas of *HBZ*-Tg mice.
doi:10.1371/journal.ppat.1001274.g002

HBZ directly induces Foxp3 expression in a CD4$^+$ T-cell intrinsic manner

To study whether HBZ increases Foxp3$^+$ T_{reg} cells in a cell intrinsic manner, we expressed HBZ in naive CD4$^+$ T cells *in vitro* using a retrovirus vector (Figure 4A). Interestingly, HBZ induced Foxp3 expression in 16.8% of HBZ expressing T cells, which is a similar enhancement to that due to TGF-β treatment (14.8%). The expression was markedly augmented in HBZ expressing T cells treated with TGF-β (72.2%) (Figure 4B). A reporter assay using the enhancer and promoter of the *Foxp3* gene [34] demonstrated that HBZ induced transcription of the *Foxp3* gene (Figure 4C), which was enhanced in the presence of TGF-β. Thus, HBZ-induced Foxp3 expression could be a mechanism for the increase of Foxp3$^+$ T cells in *HBZ*-Tg mice.

HBZ physically interacts with Foxp3

Previous studies have shown that Foxp3 controls T_{reg} function by cooperating with transcription factors including NFAT [35] and AML-1/Runx1[36]. Impaired interactions of Foxp3 with these factors not only alter the suppressive function of T_{reg} cells but also suppress the expression of T_{reg} associated molecules, such as CD25, CTLA-4, and GITR [23,35,36,37], which is similar to the

Table 1. Characteristics of lymphomas in *HBZ*-Tg and non-Tg littermates.

			Latency		IHC		
Genotype	**Strain**	**ID**	**(Months)**	**B220**	**CD3**	**Foxp3**	**Phenotype**
non-Tg			24	-	-	-	non-T, non-B
(2/27)			24	+	-	-	B
			26	+	-	-	B
			13	-	-	-	non-T, non-B
			27	-	+	+	T
			32	-	+	+	T
HBZ-Tg	#2	1	11	-	+	++	T
(14/37)	(3/14)	2	19	-	+	-	T
		3	24	-	+	+	T
	#9	1	23	+	+	+	T
	(4/5)	2	18	+	+	++	T
		3	26	+	+	+	T
		4	29	-	+	+	T
	#12	1	23	-	±	++	T
	(7/18)	2	19	-	+	+	T
		3	5	-	+	+++	T
		4	10	-	+	++	T
		5	27	+	+	-	T
		6	24	-	±	++	T
		7	18	-	+	+	T

Mice that died or became immobilized were subjected to autopsy. Tissue samples were surgically removed, fixed in 10% formalin in phosphate buffer, embedded in paraffin and stained with hematoxylin and eosin for histopathological examination. Tissue samples with lymphoma were subjected to immunohistochemical analysis (IHC) using monoclonal antibodies for CD3 (500A2), B220 (RA3-6B2), and Foxp3 (FJK-16s). The phenotype of lymphomas was determined based on CD3 and B220 expression. The degree of Foxp3 expression in lymphomas was evaluated by immunohistochemistry. (+, 1–9%; ++, 10–20%; +++, more than 20%) Frequency of T-cell lymphoma of each line is shown as follows; (number of T-cell lymphoma/number of total observed mice).

doi:10.1371/journal.ppat.1001274.t001

phenotype observed in *HBZ*-Tg mice (Figure 3, B and E). These findings prompted us to assess the possibility that HBZ might be involved in Foxp3-dependent transcriptional regulation. To address this, we first examined direct interaction among HBZ, NFAT and Foxp3. Immunoprecipitation experiments showed that HBZ physically interacted with both NFAT and Foxp3 (Figure 5A). Moreover, to study the interaction of endogenous HBZ and Foxp3, we performed immunoprecipitation using ATL-43T, a Foxp3-expressing ATL cell line. An anti-HBZ antibody co-precipitated endogenous Foxp3 in the ATL-43T cells, demonstrating that the interaction occurs not only in an enforced over-expressed state but also under physiological conditions (Figure 5B). It has been previously reported that human FoxP3 protein migrates as a doublet, which coincides with this result [38]. Analyses using HBZ deletion mutants showed that the central domain of HBZ interacted with Foxp3 (Figure 5C). Experiments with Foxp3 deletion mutants revealed that HBZ interacted with the forkhead (FH) domain of Foxp3 (Figure 5D). It has been reported that the region between the forkhead domain and the leucine zipper domain of Foxp3 interacted with AML-1 [36]. HBZ did not inhibit the binding between Foxp3 and AML-1 nor the suppressive effect of Foxp3 on AML-1-mediated transcription from the IL-2 gene promoter (Figure S11), indicating that HBZ does not influence Foxp3/AML1 mediated gene regulation.

To study whether HBZ independently interacts with Foxp3 and NFAT or, alternatively, if these molecules form a ternary complex, we studied the effect of the DNA intercalator ethidium bromide (EtBr) on their interactions. As shown in Figure 5E, the interactions of HBZ with Foxp3 or NFAT were not affected by EtBr while the interaction between NFAT and Foxp3 was diminished by EtBr as reported previously [35]. These findings suggest that the interactions of HBZ with NFAT and Foxp3 are independent of DNA while the interaction between NFAT and Foxp3 requires the presence of DNA.

HBZ inhibits Foxp3-mediated CTLA-4 and GITR expression in CD4$^+$ T cells *in vitro*

In *HBZ*-Tg mice, the expression of T_{reg}-associated molecules including CTLA-4, GITR and CD25 was suppressed when compared with their expression in T_{reg} cells from non-Tg mice (Figure 3B and E). This finding may account for the impaired function of T_{reg} cells since these molecules, in particular CTLA-4, play a critical role in T_{reg}-mediated suppression [39]. To further study the effect of HBZ on the expression of T_{reg}-associated molecules, we transduced HBZ along with Foxp3 into naive CD4$^+$ T cells *in vitro* using retrovirus vectors (Figure 4A). HBZ expression suppressed Foxp3-induced GITR and CTLA-4 expression whereas it did not inhibit CD25 expression (Figure 6A). Expression of HBZ alone increased CD25 expression (Figure 6A), which might obscure the suppressive effect of HBZ under these conditions. Suppression of GITR and CTLA-4 expression required both the activation and the central domains of HBZ (Figure 6, B and C), which correspond to the binding sites of HBZ to Foxp3 (Figure 5C) and NFAT (Figure S12). Since both Foxp3 and NFAT are critical

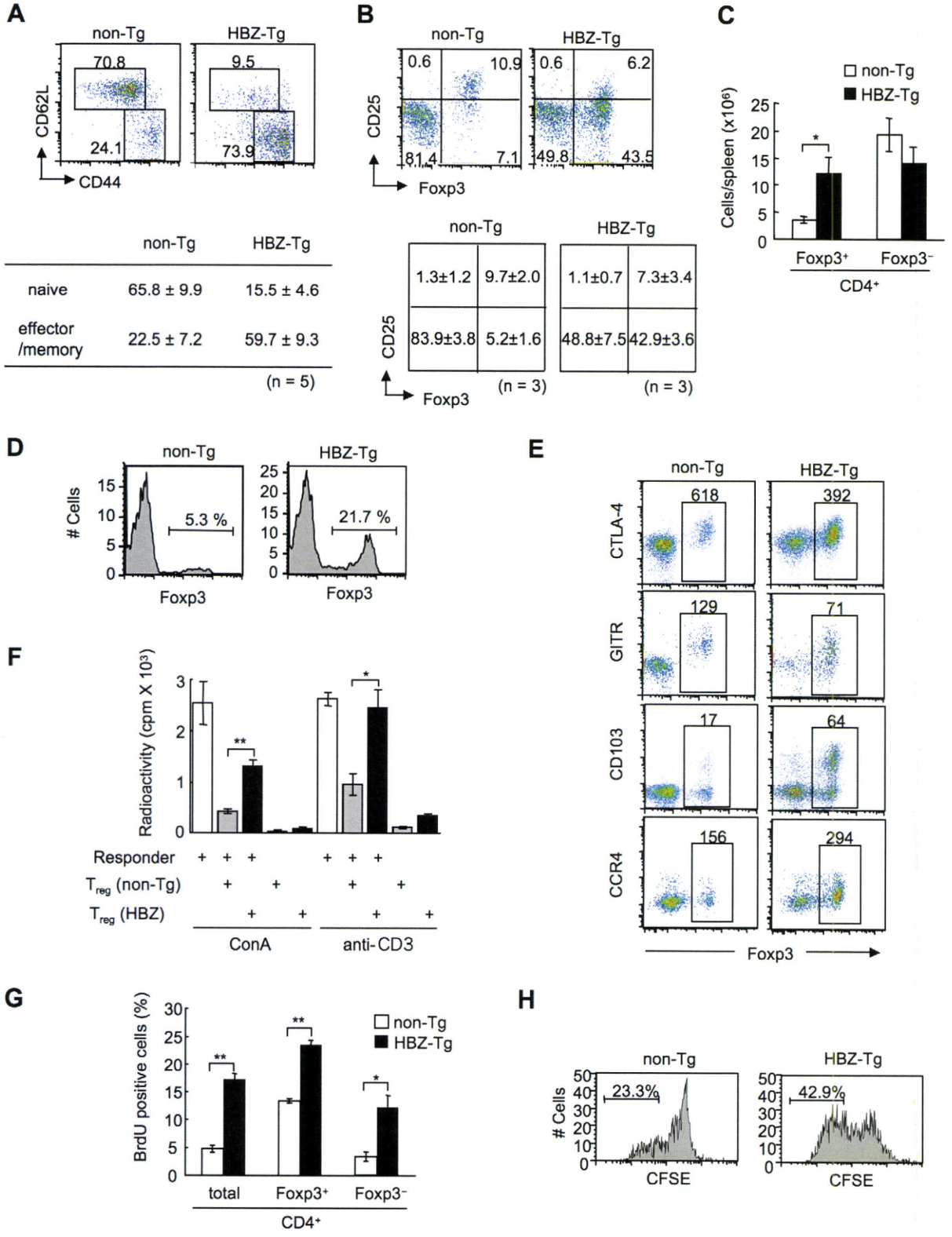

	non-Tg	HBZ-Tg
naive	65.8 ± 9.9	15.5 ± 4.6
effector /memory	22.5 ± 7.2	59.7 ± 9.3
	(n = 5)	

CD25 \ Foxp3	non-Tg		HBZ-Tg	
	1.3±1.2	9.7±2.0	1.1±0.7	7.3±3.4
	83.9±3.8	5.2±1.6	48.8±7.5	42.9±3.6
	(n = 3)		(n = 3)	

Figure 3. Transgenic expression of HBZ in CD4⁺ T cells increases Foxp3⁺ T_{reg} cells with impaired suppressive function. (A and B) Mouse splenocytes were stained with the indicated antibodies, and analyzed by flow cytometry. Representative dot plots gated on the CD4⁺ population are shown. For these experiments, *HBZ*-Tg mice without any symptoms were used. Tables show the mean ± SD (n = 5 for A, n = 3 for B). (C) The absolute number of Foxp3⁺ or Foxp3⁻ CD4⁺ T cells in *HBZ*-Tg and non-Tg mice. The results shown are the mean ± SD (n = 3). (D) Flow cytometric analysis for the Foxp3 expression in CD4 single positive thymocytes. Representative dot plots gated on the CD4 single positive population are shown from three independent analyses. (E) Flow cytometric analyses of CD4⁺ T cells for T_{reg} related molecules. Numbers in dot plots indicate mean fluorescence intensity (MFI) of each molecule in the rectangular gates. (F) Suppressive activity of T_{reg} cells from *HBZ*- or non-Tg mice on T-cell proliferation. Sorted Foxp3⁺ T cells were cultured with CD4⁺CD25⁻ cells of non-Tg mice as responder cells for 72 h with ConA or soluble anti-CD3

antibody and x-irradiated antigen presenting cells (APCs), and [^{3}H] thymidine incorporation during the last 6 hours was measured. Results are means ± SD for triplicate cultures. (G) *In vivo* BrdU incorporation in total CD4$^+$, Foxp3$^+$CD4$^+$, or Foxp3$^-$CD4$^+$ T cells. The results shown are the mean ± SD (n = 3). (H) Sorted Foxp3$^+$ cells were labeled with CFSE and cultured with anti-CD3 antibody and x-irradiated APCs. After 96 hours, the cells were stained with anti-Foxp3, and CFSE dilution was analyzed for Foxp3$^+$ cells. *, $P<0.01$; **, $P<0.001$ by two-tailed Student *t*-test.
doi:10.1371/journal.ppat.1001274.g003

for T_{reg} function [35], it is likely that HBZ suppresses the expression of GITR and CTLA-4 by interacting with Foxp3 and NFAT and thereby interfering with their transcriptional regulation in T_{reg} cells. To examine suppressive effect of HBZ on expression of GITR, CTLA-4 and CD25, we isolated T_{reg} cells from wild type mice and expressed HBZ using retroviral vectors. As shown in Figure 6D, HBZ suppressed endogenous expression of CD25, GITR and CTLA-4 in T_{reg} cells, confirming that HBZ is responsible for suppressed expression of these molecules.

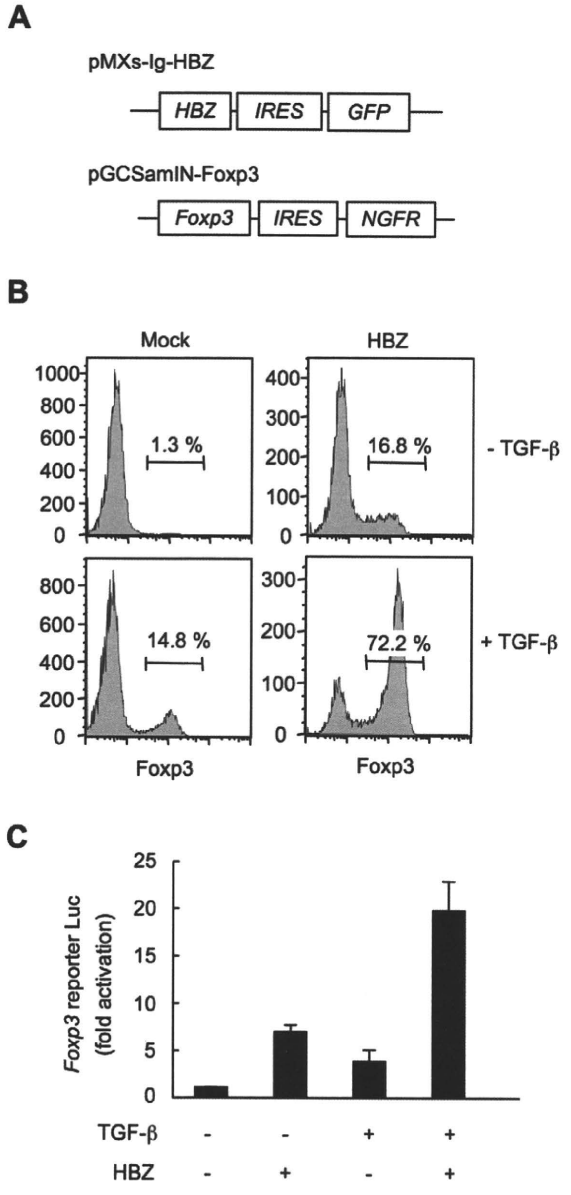

Figure 4. HBZ directly induces Foxp3 expression in CD4$^+$ T cells. (A) Schematic diagrams of retrovirus vectors used in this study. (B) Mouse CD4$^+$CD25$^-$ T cells transduced with retrovirus vector encoding HBZ or empty vector with or without TGF-β were stained with anti-Foxp3 antibody and analyzed by flow cytometry. (C) To study the effect of HBZ on promoter activity of the *Foxp3* gene, EL4 cells were transfected with Foxp3 reporter plasmid and/or HBZ expressing plasmid. Representative data shown are firefly luciferase activities normalized to those of renilla luciferase (mean ± SD).
doi:10.1371/journal.ppat.1001274.g004

Discussion

HTLV-1 targets CD4$^+$ T cells; cell central to immune regulation. In contrast to human immunodeficiency virus, which destroys CD4$^+$ T cells, HTLV-1 increases its copy number by inducing clonal proliferation of infected cells *in vivo* [40,41]. Since HTLV-1 spreads mainly by cell-to-cell transmission [5], increased number of infected cells facilitates transmission of HTLV-1 to new cells. Recent studies showed that glucose transporter 1, heparan sulfate proteoglycans and neuropilin-1 are important for the entry of HTLV-1[42,43,44], consistent with the finding that this virus can infect a variety of cell types [45,46]. However, HTLV-1 provirus is detected mainly in the regulatory and effector/memory CD4$^+$ T cells of HTLV-1 carriers (Figure S13) [25,26,27], which indicates that HTLV-1 favors these specific subpopulations of CD4$^+$ T cells. These findings suggest that HTLV-1 induces proliferation and/or facilitates survival of the regulatory and effector/memory CD4$^+$ T cells. The mechanism(s) by which HTLV-1 targets T_{reg} cells, however, remained unclear until now. In this study, we showed that HBZ could enhance transcription of the *Foxp3* gene, and also promote proliferation of Foxp3$^+$CD4$^+$ T cells in transgenic mice, indicating that HBZ enhances both the generation and proliferation of Foxp3$^+$ T cells. Impaired Foxp3 function is associated with proliferation of T_{reg} cells [37], so the HBZ-mediated T_{reg} dysfunction may also contribute to T_{reg} proliferation in addition to direct growth proliferation by the HBZ transcript [13]. Another possible explanation is that T_{reg} cells might be more susceptible to HTLV-1 infection, since T_{reg} cells proliferate vigorously *in vivo* presumably by recognizing self-antigen and commensal microbes [47]. With these strategies, HTLV-1 likely targets this specific T-cell population as its host, which might be beneficial for their survival.

As mechanisms of the HBZ-mediated effect on Foxp3 functions, we demonstrated that HBZ physically interacted with Foxp3 and impaired its function *in vitro*. HBZ lacking the Foxp3-binding region showed a slight inhibitory effect on Foxp3 function, indicating that direct interaction between HBZ and Foxp3 is, at least in part, responsible for suppression. The results of immunoprecipitation analyses using Foxp3 mutants showed that the forkhead domain of Foxp3 was responsible for the molecular interaction between HBZ and Foxp3. Since the forkhead domain is the DNA-binding domain of Foxp3 [17], HBZ might inhibit the transcriptional function of Foxp3 by interfering with the DNA binding activity. Foxp3 play a key role in the function and homeostasis of T_{reg} cells [22,23,24], indicating that HBZ-mediated dysfunction of Foxp3 contributes to impaired T_{reg} function in *HBZ*-Tg mice. This impaired T_{reg} function allows non-regulatory T cells to become hyper-reactive to commensal microbes and self-antigens, provoking enhanced proliferation of non-regulatory T cells and T cell-mediated autoimmune/inflammatory disease. These data collectively suggest that the viral protein HBZ hijacks the transcriptional

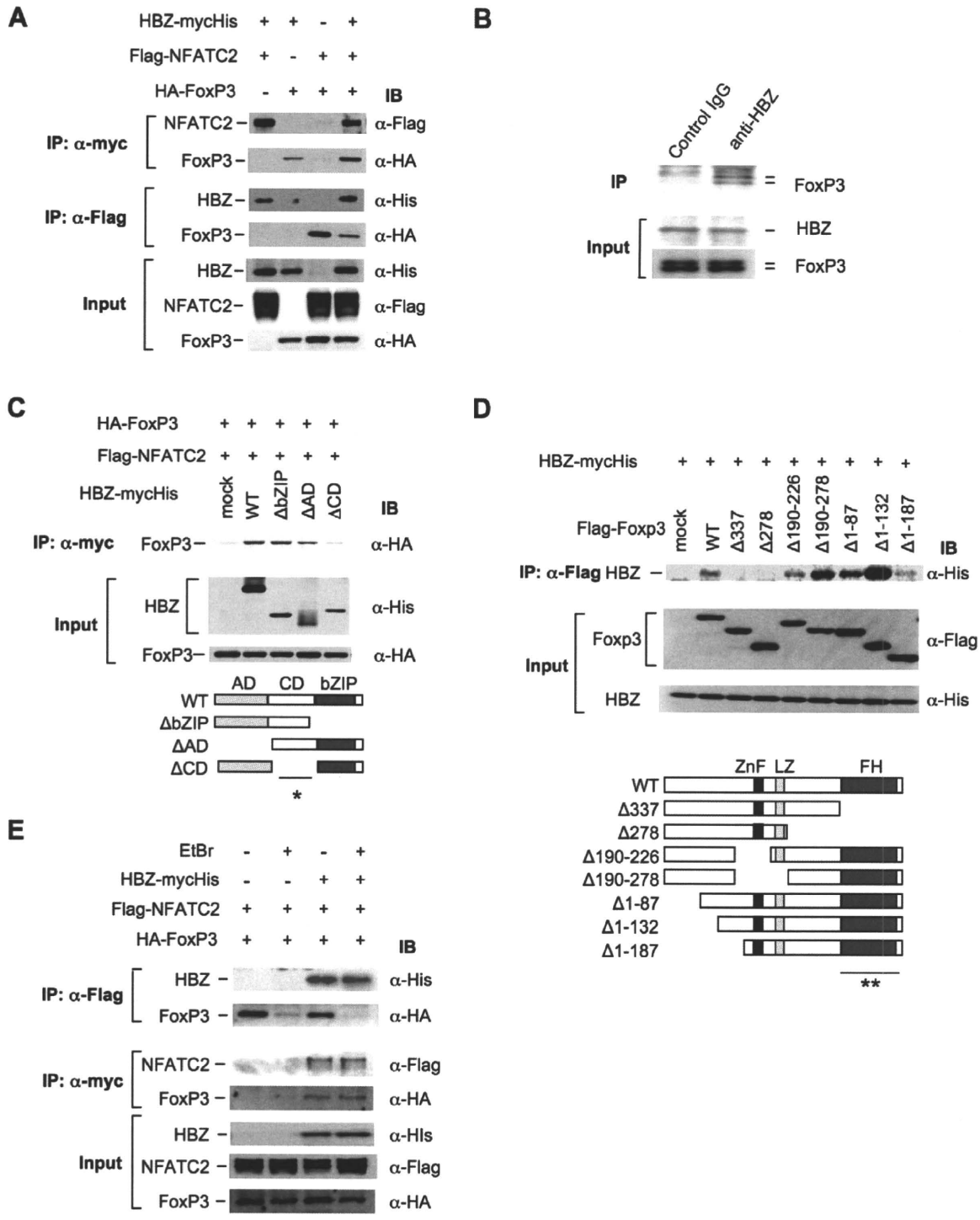

Figure 5. HBZ physically interacts with Foxp3 and NFAT. (A) The expression vectors of the indicated proteins were co-transfected into 293FT cells, and their interactions were analyzed by immunoprecipitation (IP). (B) Nuclear extract of ATL-43T cells was subjected to IP with anti-HBZ antibody or control IgG, and detected by anti-FoxP3 antibody. (C and D) The interactions of HBZ and Foxp3 were analyzed by IP using HBZ mutants (C) or Foxp3 mutants (D). A schematic diagram of Foxp3 mutants is shown. ZnF, zinc finger; LZ, leucine zipper; FH, forkhead domain. Asterisks (* or **) show responsible region for each molecular interaction. (E) The interactions among HBZ, Foxp3 and NFATc2 were analyzed with or without EtBr.
doi:10.1371/journal.ppat.1001274.g005

machinery of host T_{reg} cells leading to inflammatory disorders in the host. Conversely, Tax, another HTLV-1 protein, has been reported to suppress FoxP3 expression in human T cells *in vitro* [48]. Therefore, it is likely that both viral proteins target Foxp3 albeit with apparently different effects. Considering that HBZ is consistently expressed while Tax expression is sporadic, Tax might control excess expression of Foxp3 in HTLV-1 infected cells.

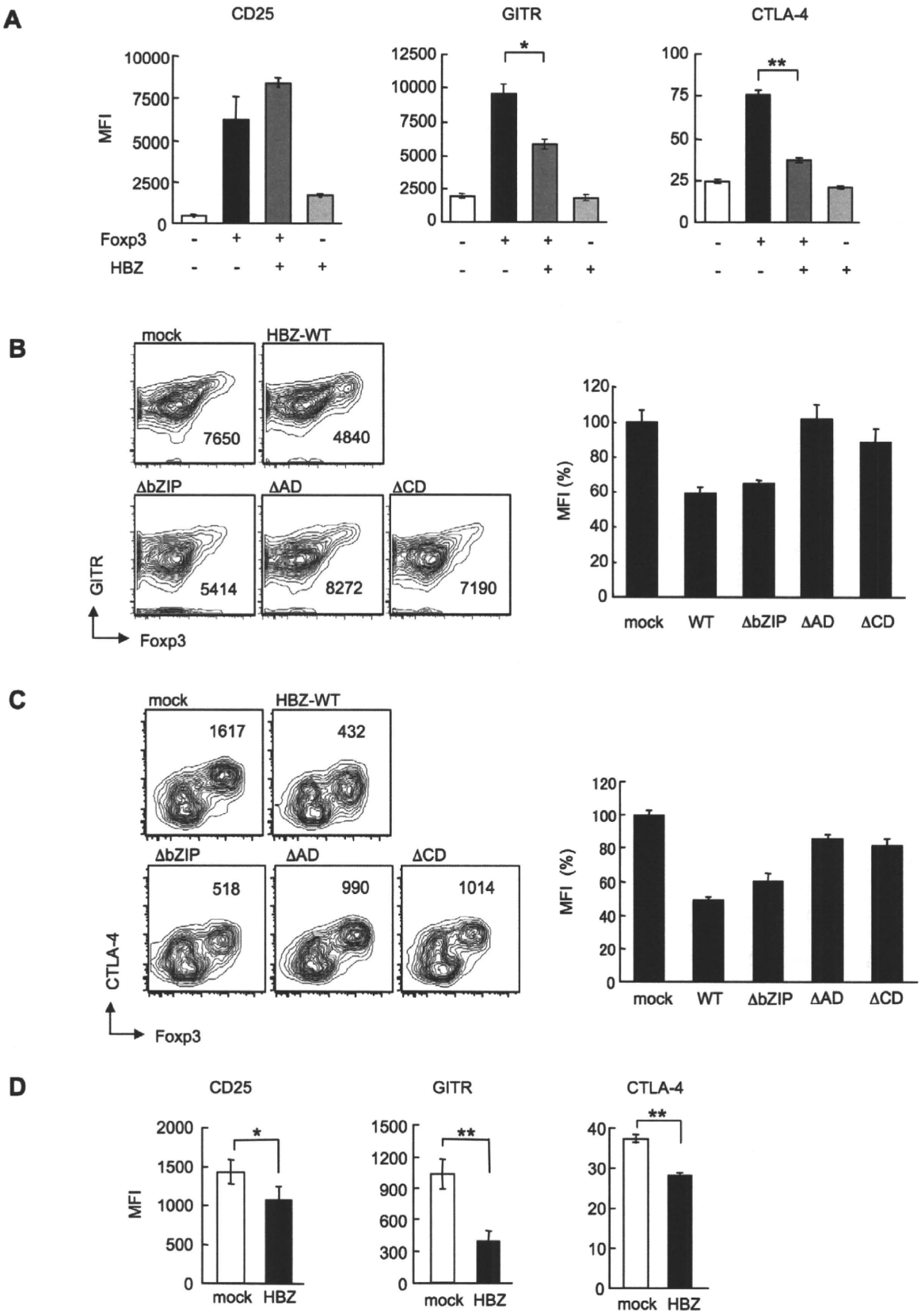

Figure 6. HBZ inhibits Foxp3-mediated CTLA-4 and GITR expression *in vitro*. (A) Mouse $CD4^+CD25^-$ T cells co-transduced with the retroviral vectors were stained with the indicated antibodies. Mean fluorescence intensity (MFI) of CD25, GITR, and CTLA-4 in GFP/NGFR double-positive cells are shown as mean ± SD. for triplicate culture. *, $P<0.01$; **, $P<0.001$ by two-tailed Student *t*-test. (B and C) $CD4^+CD25^-$ T cells transduced with the pMXs-Ig vector encoding wild-type or mutant HBZ, and pGCSamIN-Foxp3 vector were stained with anti-GITR (B) or anti-CTLA-4

(C) antibody in addition to anti-NGFR antibody, and then analyzed by flow cytometry. *Left*, numbers in density plots indicate MFI of GITR (B) or CTLA-4 (C) in GFP/NGFR double-positive cells. Representative data from three independent experiments are shown. *Right*, relative MFI of wild type or mutated HBZ compared to mock transduced cells was shown as mean ± SD (n = 3). (D) HBZ transduction in Foxp3$^+$ T_{reg} cells inhibited the endogenous expression of T_{reg} associated molecules. Mean fluorescence intensity (MFI) of CD25, GITR, and CTLA-4 in CD4$^+$Foxp3$^+$NGFR$^+$ cells are shown as mean ± SD. for triplicate culture. *, $P<0.05$; **, $P<0.01$ by two-tailed Student *t*-test.
doi:10.1371/journal.ppat.1001274.g006

In this study, we demonstrated that the characteristics of CD4$^+$ T cells in *HBZ*-Tg mice resemble those of human ATL cells or HTLV-1 infected cells in carriers. First, the frequency of Foxp3 positive cells in T-cell lymphomas was similar in *HBZ*-Tg mice and in ATL [20]. Second, the suppressive function of Foxp3$^+$ T cells was impaired in both ATL and *HBZ*-Tg mice [49]. Third, CD4$^+$ T cells in *HBZ*-Tg mice, HTLV-1-infected cells in carriers, and ATL cells possess similar effector/memory and regulatory phenotypes [25,27]. As shown in this study, transgenic mice expressing Tax under the same promoter as the *HBZ*-Tg mice did not show any changes in the number of Foxp3$^+$ T_{reg} cells or effector/memory T cells. These data suggest that HBZ, rather than Tax, is responsible for conferring the specific phenotype of HTLV-1 infected cells and ATL cells.

It has been reported that *tax* transgenic animals develop tumors [50,51,52]. In these reports, Tax induced tumors, the type of which depends on the promoter used. However, irrespective of the possible oncogenic activity of Tax, leukemic cells in ATL patients frequently lose Tax expression [7], whereas *HBZ* expression has been detected in all ATL cases studied so far [13]. We reported that the *HBZ* gene transcript itself has growth-promoting activity *in vitro* [13]. Taken together, our results suggest that HBZ is responsible for the specific phenotype, function and proliferation of HTLV-1-infected CD4$^+$ T cells and ATL cells, and that HBZ plays important roles for the oncogenic activity of HTLV-1 in addition to Tax. Further, the long latent period before the onset of T-cell lymphomas in *HBZ*-Tg mice suggests that additional genetic and/or epigenetic alterations in CD4$^+$ T cells are necessary for the development of T-cell lymphomas in *HBZ*-Tg mice as well as for ATL.

In conclusion, the HBZ-mediated dysregulation of T_{reg} function and proliferation that we report here provides novel insights into the interaction between the host and the virus and may be exploited to treat and prevent HTLV-1-induced diseases.

Materials and Methods

Ethics statement

This study was conducted according to the principles expressed in the Declaration of Helsinki. The study was approved by the Institutional Review Board of Kyoto University (E921). All patients provided written informed consent for the collection of samples and subsequent analysis. Animal experimentation was performed in strict accordance with the Japanese animal welfare bodies (Law No. 105 dated 19 October 1973 modified on 2 June 2006), and the Regulation on Animal Experimentation at Kyoto University. The protocol was approved by the Institutional Animal Research Committee of Kyoto University (Permit Number: D09-3). All efforts were made to minimize suffering.

Mice and cell cultures

C57BL/6J mice were purchased from CLEA Japan. The HBZ cDNA was cloned into the *SalI* site of the H/M/T-CD4 vector, which was designed for restricted expression of a transgene in CD4$^+$ cells. The purified fragment containing the HBZ transgene was microinjected into C57BL/6J F1 fertilized eggs. Transgenic founders were screened for the integration of transgenes in their genomic DNA by PCR and mated with C57BL/6J mice to generate transgenic progeny [13,15]. All *HBZ*-Tg mice were heterozygotes for the transgene. The phenotype of *HBZ*-Tg mice was stable in the different generations. They express the spliced *HBZ* gene under the control of the *CD4*-specific promoter/enhancer/silencer. All mice were used at 10-16 weeks of age unless specifically described.

The human embryonic kidney cell line, 293FT, was cultured in DMEM containing 10% FCS and G418 (500 μg/ml). The 293FT cell line is derived from the 293F cell line and stably expresses the SV40 large T antigen. 293FT cell line was purchased from Invitrogen. The packaging cell line, Plat-E (kindly provided by T. Kitamura, Tokyo University) was cultured in DMEM supplemented with 10% FCS containing 10 μg/ml blasticidin and 1 μg/ml puromycin. ATL-43T(−) (kindly provided by M. Maeda, Kyoto University) and MT-1 cells were derived from ATL cells, and cultured in RPMI containing 10% FCS and antibiotics (penicillin and streptomycin). A mouse T-cell lymphoma line, EL4 cells, were cultured with RPMI1640 containing 10% FCS, antibiotics, and 50 μM 2-mercaptoethanol (2-ME; Invitrogen).

Plasmids

In order to construct the vectors expressing tagged spliced HBZ and its mutants, their coding sequences were amplified by PCR, and cloned into the expression vector, pcDNA 3.1(−)/myc-His (Invitrogen). A cDNA clone that contains NFATc2 coding sequence was kindly provided by Kazusa DNA Research Institute. To construct the FLAG-tagged NFATc2 expression vector, its coding region was cloned into pCMV-Tag2 (Stratagene). pCMV-HA (Clontech) was used to generate HA-tagged Foxp3 expression vectors. The vectors expressing Flag-tagged Foxp3 mutants were also used for immunoprecipitation.

Antibodies and reagents

The following antibodies were used for immunoprecipitation and Western blotting: mouse anti-Flag (clone M2; Sigma, Saint Louis, MO), mouse anti-c-myc (clone 9E10; Sigma), mouse anti-HA (clone HA-7; Sigma), rabbit anti-His polyclonal antibody (MBL), rabbit anti-FOXP3 (polyclonal antibody; Abcam), and rabbit anti-HBZ polyclonal antisera [15].

The following antibodies were purchased from BD PharMingen; purified monoclonal antibody (mAb) for mouse CD4 (RM4-5), CD8α (53-6.7), CD25 (PC61), CD44 (IM7), CD103 (M290), and IL-2 (JES6-5H4). Purified monoclonal antibodies for mouse GITR (DTA-1), CTLA-4 (UC10-4B9), CD62L (MEL-14), TCRβ (H57-597), TCRγδ (eBioGL3) and Foxp3 (FJK-16s) or human FoxP3 (236A/E7) were purchased from eBioscience. Anti-mouse CCR4 antibody (polyclonal antibody; Capralogics) and FITC-labeled anti-goat IgG antibody (Santa Cruz Biotechnology) were used for the detection of mouse CCR4. The following reagents were used for cell culture: anti-CD3ε antibody (145-2C11; R&D systems), Con A (Sigma), PMA (Sigma), and ionomycin (Sigma).

Synthesis of cDNA and semiquantitative RT-PCR

cDNAs were synthesized from 1 μg total RNA of purified mouse CD4$^+$ T cells by a reverse transcriptase SuperScript III and random primers according to the manufacturer's instructions

(Invitrogen). Spliced *HBZ* and *GAPDH* transcripts were quantified using RT-PCR. The primers used were as follows: s*HBZ* gene: 5′-TAAACTTACCTAGACGGCGG-3′ (sense), 5′-CTGCCGATCACGATGCGTTT -3′ (antisense); *GAPDH* gene: 5′-GTGGAGA TTGTTGCCATCAACG -3′ (sense) and 5′-AGAGGGGCCATCCACAGTCTT-3′ (antisense). PCR was performed in a PC-808 (Astec) under the following conditions: *HBZ*: 2 minutes at 95°C, followed by 26 cycles of 30 seconds at 95°C, 30 seconds at 59°C and 60 seconds at 72°C; *GAPDH:* 3 minutes at 95°C, followed by 35 cycles of 30 seconds at 95°C, 30 seconds at 61°C and 30 seconds at 72°C.

Quantitative RT-PCR

To quantify the expression level of *HBZ*, a TaqMan probe and primers for *HBZ* were designed. The sequences of primers and probe for *HBZ* were as follows; *HBZ* primers; 5′-GGACGCAGTTCAGGAGGCAC-3′ (sense) and 5′-CCTCCAAGGATAATAGCCCG-3′ (antisense); *HBZ* probe; 5′-CCTGTGCCATGCCCGGAGGACCTGC-3′. We used the TaqMan Gene expression Assay for *18S rRNA* (Applied Biosystems) as an internal control. Relative expression level of *HBZ* or *IL-2* was calculated with the delta delta Ct method.

Retroviral constructs and transduction

For retroviral gene transduction experiments, spliced HBZ cDNA was cloned into a retroviral vector, pMXs-Ig (a gift from T. Kitamura), to generate pMXs-Ig-HBZ. pGCSamIN (kindly provided from M. Onodera) and pGCSamIN-Foxp3 were used as previously described. Transfection of the packaging cell line, Plat-E, was performed as described. For retroviral transduction, $CD25^{-}CD4^{+}$ cells were enriched by a CD4 enrichment kit (BD Pharmingen) and were activated by 0.5 μg/ml anti-CD3 Ab and 50 U/ml rIL-2 in the presence of T-cell-depleted and x-irradiated (20Gy) C57BL/6J splenocytes as APCs in 12 well plates. After 16 hours, activated T cells were transduced with viral supernatant and 4 μg/ml polybrene, and centrifuged at 3,000 rpm for 60 min. Cells were cultured in medium supplemented with 50 U/ml rIL-2. Activation of naïve T cells by anti-CD3 antibody influenced expression of these molecules. Therefore, we analyzed their expression after influence by activation was lost [35]. Two days later, Foxp3-mediated CTLA-4 expression was detected by a flow cytometry, and five days later, expression of GITR or CD25 was analyzed. After two days, we stimulated the transduced cells with 50 ng/ml PMA and 1 μg/ml ionomycin in the presence of protein transport inhibitor (BD PharMingen) for 6 hours, and then analyzed intracellular IL-2 expression using intracellular cytokine staining kits (BD Pharmingen) according to the manufacturer's instructions.

To elucidate the effect of HBZ on endogenous expression of T_{reg} associated molecules, we transduced HBZ into $CD4^{+}Foxp3^{+}$ cells purified from mouse splenocytes. Three days after transduction, the expression levels of T_{reg} associated molecules were evaluated by a flow cytometry.

Preparation of splenocytes, flow cytometric analyses, cell sorting, and assays of regulatory T cells

Cell suspensions were prepared from murine spleens by forcing the organs through a nylon mesh, and splenic erythrocytes were eliminated with NH_4Cl. Proliferation of murine cells was measured by ^{3}H-thymidine uptake after 3 days of incubation in RPMI1640 medium supplemented with 10% FCS and 50 μM 2-ME. Flow cytometric analyses and cell sorting were carried out using a FACS CantoII or FACS Aria with Diva Software (BD Pharmingen) and the data was analyzed by FlowJo software (Treestar). For cell surface staining, 10^{6} cells were incubated with mAbs for 30 min at 4°C, and then analyzed. For intracellular staining, we used a mouse Foxp3 staining kit according to its protocol (eBioscience). To sort $Foxp3^{+}$ cells, suspended splenocytes were stained with mAb for CD4 and GITR, and the $CD4^{+}GITR^{high}$ fraction was sorted by FACS Aria. Purity of the sorted population was always >90% by re-analysis of Foxp3 staining. For the *ex vivo* proliferation assay of $Foxp3^{+}$ cells, carboxyfluorescein diacetate, succinimidyl ester (CFSE)(Molecular Probe) was used according to the manufacturer's instructions. $Foxp3^{+}$ T cells (2×10^{4}/well) were stimulated with anti-CD3 antibody (4 μg/ml) in round-bottomed 96-well plates in the presence of x-irradiated splenocytes as antigen presenting cells (APC; 5×10^{4}/well) for 96 hours. Then, cells were permeabilized, and stained with anti-Foxp3. CFSE dilution was analyzed by flow cytometry. To evaluate the suppressive activity of $Foxp3^{+}$ T cells sorted from *HBZ*-Tg or non-Tg mice, $Foxp3^{+}$ T cells (2×10^{4}/well) were cultured with $CD25^{-}CD4^{+}$ cells (2×10^{4}/well) and APCs (5×10^{4}/well) from wild-type mice for 72 h in the presence of soluble anti-CD3 (4 μg/ml) or Con A (1 μg/ml), and then $[^{3}H]$ thymidine incorporation was measured.

BrdU staining

In vivo proliferation was measured by BrdU incorporation. BrdU (Nacalai Tesque) was dissolved in PBS (3 μg/ml), and then 200 μl was injected intraperitoneally into *HBZ*-Tg and non-transgenic mice twice a day for three days as reported previously [53]. BrdU incorporation in $CD4^{+}$, $CD8^{+}$, or $B220^{+}$ splenocytes was detected using FITC BrdU Flow Kits (BD Pharmingen) according to the manufacturer's instructions. Flow cytometric analyses were performed on a FACS CantoII with Diva Software (BD Pharmingen).

Foxp3 reporter assay

We constructed Foxp3 promoter and enhancer reporter plasmids as the previous report [34]. A murine T-cell line, EL4 cells (1×10^{7}), were transiently cotransfected by electroporation with the following plasmid DNAs: *Foxp3* reporter plasmid, *Renilla* luciferase control vector (pRL-TK), and HBZ expression vector (pME18SneoHBZ). Cells were cultured with or without TGF-β (2 ng/ml). Firefly and *Renilla* luciferase activities were measured using the Dual-Luciferase Reporter Assay System (Promega). Relative luciferase activities were calculated as the ratio of firefly and *Renilla* luciferase activities. The luciferase values are shown as relative values. Values represent means plus standard deviations (error bars) (n = 3).

Histological analyses

The study of clinical samples was approved by the local research ethics committee of the appropriate hospital. Tissue samples were fixed in 10% formalin in phosphate buffer and then embedded in paraffin. Haematoxylin and eosin (H&E) staining was performed according to standard procedures. Images were captured using a Provis AX80 microscope (Olympus) equipped with OLYMPUS DP70 digital camera, and detected using a DP manager system (Olympus).

For analysis of tumors, mice that became immobilized were sacrificed and subjected to autopsy. Tissue samples were surgically removed and fixed in 10% formalin in phosphate buffer and embedded in paraffin. Sections were stained with H&E for histopathologic examination. After we obtained informed consent, tissue samples from patients who were diagnosed as lymphoma-type ATL were analyzed by immunohistochemical methods to

determine FoxP3 expression. Monoclonal antibodies for CD3ε(500A2; BD Pharmingen), B220 (RA3-6B2; BD Pharmingen), and Foxp3 (FJK-16s; eBioscience) were used for immunohistochemistry. We judged $CD3^+B220^+$ cases to be T-cell lymphomas since some activated T cells and T cells of the *lpr/lpr* mutant mouse expressed B220 [54,55].

PCR/single stranded conformation polymorphism (SSCP) analysis

To investigate clonality of lymphoma cells observed in *HBZ*-Tg mice, lymphoma tissue samples of *HBZ*-Tg were analyzed for the clonality of T-cell receptor (TCR) γ locus using PCR-SSCP analysis of the TCR γ-gene. Genomic DNA was subjected to PCR amplification using primers for the Vγ2 gene and the Jγ1. The primers used were as follows: Vγ2: 5′-ACCAAGAGATGAGACTGCACAA-3′ (sense), Jγ1: 5′-GCGTCTGATCCTCAAAATAACTTCC-3′ (antisense); PCR was performed in a PC-808 (Astec) under the following conditions: 3 minutes at 95°C, followed by 35 cycles of 30 seconds at 95°C, 30 seconds at 55°C and 30 seconds at 72°C. We used EL-4 as a positive control and splenic DNA from young non-Tg or *HBZ*-Tg mice as negative control. PCR products were run on a 6% polyacrylamide gel and visualized by staining with DNA Silver Staining Kit (GE Healthcare).

Coimmunoprecipitation assay and immunoblotting

Expression vectors for the relevant genes were transiently cotransfected into 293FT cells using the TransIT-LT1 reagent (Mirus Bio). 24 hours later, transfected cells were stimulated with 50 ng/ml PMA and 1 μg/ml ionomycin for another 6 hours. Coimmunoprecipitation assays were performed using the Nuclear Complex Co-IP Kit (Active motif). Briefly, the nuclear extracts of transfected cells were prepared in the presence or absence of ethidium bromide (10 μg/ml). They were precleared with Protein G Sepharose 4 Fast Flow (GE Healthcare), and their supernatants were incubated with anti-myc tag (clone 9E10, Sigma) or anti-Flag tag (M2, Sigma) antibody overnight at 4°C. The immunocomplexes were precipitated with Protein G Sepharose 4 Fast Flow, fractionated in SDS-PAGE, and transferred to PVDF membranes. HBZ-myc-His was detected with horseradish peroxidase (HRP)-conjugated anti-His tag (MBL) antibody. HRP-conjugated anti-Flag tag (Sigma) and anti-HA tag (Sigma) antibodies were used to detect Flag-tagged and HA-tagged proteins, respectively. To detect endogenous interaction between HBZ and FoxP3, immunoprecipitation was performed using an ATL cell line, ATL-43T (-), as described above with anti-HBZ antisera and anti-FOXP3 antibody (Abcam). To examine the expression of HBZ in transgenic mice, $CD4^+$ splenocytes from wild type or *HBZ*-Tg mice were enriched by a mouse CD4 T lymphocyte enrichment set (Pharmingen). Whole cell extracts were prepared with the lysis buffer (50 mM Tris-HCL, PH 7.5, 150 mM NaCl, 1% NP-40), and analyzed by western blotting with anti-HBZ antisera.

Flow cytometric analysis for HTLV-1 carrier cells

A previous report demonstrated that Tax expression could not be detected in freshly isolated PBMC from HTLV-1 infected carriers but could be detected when they were cultivated *ex vivo* for 12 hours [56]. We cultured PBMCs from asymptomatic HTLV-1 carriers for 12 hours and stained with monoclonal antibodies against FoxP3 or Tax (MI-73), and then analyzed by flow cytometry.

Statistical analysis

For *in vitro* experiments, multiple data comparisons were performed using Student's unpaired *t*-test. Statistical differences in the incidence of T-cell lymphoma were analyzed using a logrank test.

Supporting Information

Figure S1 Characterization of the transgene. (A) Schematic structure of the transgene. (B) Copy numbers of the transgene in each line were determined by Southern blot analysis. Serially diluted plasmids, used to calculate the copy number, are shown on the left side.
Found at: doi:10.1371/journal.ppat.1001274.s001 (0.35 MB TIF)

Figure S2 Histological analysis of the skin and lung of *HBZ*-Tg mice. HE staining showed massive infiltration of lymphocytes in *HBZ*-Tg line 9 and 12, but not in line 2. Immunohistochemical staining revealed that only some of infiltrating lymphocytes were FoxP3 positive. Arrows indicate FoxP3 positive cells.
Found at: doi:10.1371/journal.ppat.1001274.s002 (4.46 MB TIF)

Figure S3 Flow cytometric analysis of TCRβ and TCR γδ expression in the spleen with lymphoma observed in *HBZ*-Tg mice. Numbers are identical to those of Table 1.
Found at: doi:10.1371/journal.ppat.1001274.s003 (0.32 MB TIF)

Figure S4 PCR/single stranded conformation polymorphism (SSCP) analysis. *HBZ*-Tg lymphoma tissue samples were analyzed for TCR clonality using PCR-SSCP analysis of the TCR γ-gene. EL-4 are shown as a positive control and splenic DNA from young (less than 6 weeks old) non-Tg or *HBZ*-Tg mice as a negative control. Lanes 1- 5 (#2-3, #9-1, #12-6, #9-3, #12-7) show lymphoma from *HBZ*-Tg mice respectively (Table 1).
Found at: doi:10.1371/journal.ppat.1001274.s004 (1.09 MB TIF)

Figure S5 Analysis of FoxP3 expression in fresh ATL cells. Immunohistochemical staining for FoxP3 in the lymph nodes of human ATL patients. We used a monoclonal antibody for human FoxP3 (236A/E7; eBioscience).
Found at: doi:10.1371/journal.ppat.1001274.s005 (1.89 MB TIF)

Figure S6 Flow cytometric analysis of thymocyte subsets. Non-Tg or *HBZ*-Tg thymocytes were stained with anti-CD4 and anti-CD8 antibody, and then analyzed by flow cytometry.
Found at: doi:10.1371/journal.ppat.1001274.s006 (0.48 MB TIF)

Figure S7 Foxp3 expression in spleen, cervical lymph node, or peripheral blood mononuclear cells was determined by flow cyotmetry. Representative histograms gated on the $CD4^+$ population are shown.
Found at: doi:10.1371/journal.ppat.1001274.s007 (0.36 MB TIF)

Figure S8 *HBZ*-Tg line 2 also showed an increase in effector/memory and regulatory CD4 T cells. Mouse splenocytes were stained with antibodies for CD4 and CD8 plus CD44 and CD62L (A) or CD25 and Foxp3 (B), and then analyzed by flow cytometry. Representative dot plots gated on the $CD4^+$ population are shown.
Found at: doi:10.1371/journal.ppat.1001274.s008 (0.57 MB TIF)

Figure S9 IL-2 production of $CD4^+$ T cells in *HBZ*-Tg mice. (A) Mouse splenocytes were stimulated with Leukocyte Activation Cocktail, which contains PMA/Ionomycin and protein transport inhibitor (BD Pharmingen), for 4 hours and then analyzed for intracellular IL-2 gated on the $CD4^+$ cells by flow cytometry. Representative results of more than three independent experiments are shown. (B) The percentage of $IL\text{-}2^+$ cells among $Foxp3^+$ cells is shown. The results shown are the mean ± SD of triplicate experiments.
Found at: doi:10.1371/journal.ppat.1001274.s009 (0.26 MB TIF)

Figure S10 Flow cytometric analyses of *tax*-Tg mice. Non-Tg or *tax*-Tg splenocytes were stained with the indicated antibodies, and analyzed by flow cytometry. Representative dot plots gated on the $CD4^+$ population are shown.
Found at: doi:10.1371/journal.ppat.1001274.s010 (0.54 MB TIF)

Figure S11 The effect of HBZ on Foxp3/AML-1 complex. (A) 293FT-cells were co-transfected with vectors expressing the indicated proteins, lysed, and subjected to immunoprecipitation. (B) Jurkat cells were co-transfected with expression vectors for the indicated proteins and IL-2 promoter-luc constructs. The results shown are relative values of firely luciferase normalized to Renilla luciferase and expressed as means ± SD. The experiments were repeated three times with similar results.
Found at: doi:10.1371/journal.ppat.1001274.s011 (0.37 MB TIF)

Figure S12 Characterization of the interaction between HBZ and NFAT. To investigate the region responsible for each interaction, we performed immunoprecipitation experiments with NFATC2 and deletion mutants of HBZ. Asterisk shows the region responsible for the molecular interaction.
Found at: doi:10.1371/journal.ppat.1001274.s012 (0.25 MB TIF)

Figure S13 The percentages of HTLV-1^+ T cells in $CD4^+FoxP3^-$ and $CD4^+FoxP3^+$ subpopulations of asymptomatic HTLV-1 carriers. It has been reported that ex vivo culture induces the reactivation of viral antigen in HTLV-1 infected cells. We cultured freshly isolated PBMC from two asymptomatic HTLV-1 carriers for 18 hours, and then stained intracellular Tax as a viral antigen to detect the presence of HTLV-1 by using a monoclonal antibody of Tax (MI-73).
Found at: doi:10.1371/journal.ppat.1001274.s013 (0.31 MB TIF)

Table S1 (A) Summary of BrdU incorporation *in vivo*. Data shown are percentage of BrdU positive cells of three different non-Tg or *HBZ*-Tg mice. (B) MFI of Treg associated molecules (CTLA-4, GITR, CD103, or CCR4) in non-Tg or *HBZ*-Tg (line 12) mice are shown as mean ± SD (n = 3). of three mice. *, $P<0.05$; **, $P<0.01$ by two-tailed Student t-test.
Found at: doi:10.1371/journal.ppat.1001274.s014 (0.25 MB TIF)

Acknowledgments

We thank A. Koito for H/M/T-CD4 vector; T. Kitamura for the pMXs-Ig vector and Plat-E cell; M. Onodera for the pGCSamIN vector; and J. Tanabe and A. Kamamoto for technical assistance, and Aaron Coutts and Kate Hayes-Ozello for editorial comments.

Author Contributions

Conceived and designed the experiments: YS JY MM. Performed the experiments: YS JY TZ MY PM KT KS KO. Analyzed the data: YS KO NO SS MM. Contributed reagents/materials/analysis tools: PLG TY MO. Wrote the paper: YS JY PLG NO SS MM.

References

1. Takatsuki K (2005) Discovery of adult T-cell leukemia. Retrovirology 2: 16.
2. Gallo RC (2005) The discovery of the first human retrovirus: HTLV-1 and HTLV-2. Retrovirology 2: 17.
3. Gessain A, Barin F, Vernant JC, Gout O, Maurs L, et al. (1985) Antibodies to human T-lymphotropic virus type-I in patients with tropical spastic paraparesis. Lancet 2: 407–410.
4. Osame M, Usuku K, Izumo S, Ijichi N, Amitani H, et al. (1986) HTLV-I associated myelopathy, a new clinical entity. Lancet 1: 1031–1032.
5. Igakura T, Stinchcombe JC, Goon PK, Taylor GP, Weber JN, et al. (2003) Spread of HTLV-I between lymphocytes by virus-induced polarization of the cytoskeleton. Science 299: 1713–1716.
6. Pais-Correia AM, Sachse M, Guadagnini S, Robbiati V, Lasserre R, et al. (2010) Biofilm-like extracellular viral assemblies mediate HTLV-1 cell-to-cell transmission at virological synapses. Nat Med 16: 83–89.
7. Matsuoka M, Jeang KT (2007) Human T-cell leukaemia virus type 1 (HTLV-1) infectivity and cellular transformation. Nat Rev Cancer 7: 270–280.
8. Journo C, Douceron E, Mahieux R (2009) HTLV gene regulation: because size matters, transcription is not enough. Future Microbiol 4: 425–440.
9. Grassmann R, Aboud M, Jeang KT (2005) Molecular mechanisms of cellular transformation by HTLV-1 Tax. Oncogene 24: 5976–5985.
10. Lairmore MD, Silverman L, Ratner L (2005) Animal models for human T-lymphotropic virus type 1 (HTLV-1) infection and transformation. Oncogene 24: 6005–6015.
11. Larocca D, Chao LA, Seto MH, Brunck TK (1989) Human T-cell leukemia virus minus strand transcription in infected T-cells. Biochem Biophys Res Commun 163: 1006–1013.
12. Gaudray G, Gachon F, Basbous J, Biard-Piechaczyk M, Devaux C, et al. (2002) The complementary strand of the human T-cell leukemia virus type 1 RNA genome encodes a bZIP transcription factor that down-regulates viral transcription. J Virol 76: 12813–12822.
13. Satou Y, Yasunaga J, Yoshida M, Matsuoka M (2006) HTLV-I basic leucine zipper factor gene mRNA supports proliferation of adult T cell leukemia cells. Proc Natl Acad Sci U S A 103: 720–725.
14. Fan J, Ma G, Nosaka K, Tanabe J, Satou Y, et al. (2010) APOBEC3G generates nonsense mutations in human T-cell leukemia virus type 1 proviral genomes in vivo. J Virol 84: 7278–7287.
15. Arnold J, Zimmerman B, Li M, Lairmore MD, Green PL (2008) Human T-cell leukemia virus type-1 antisense-encoded gene, Hbz, promotes T-lymphocyte proliferation. Blood 112: 3788–3797.
16. Saito M, Matsuzaki T, Satou Y, Yasunaga J, Saito K, et al. (2009) In vivo expression of the HBZ gene of HTLV-1 correlates with proviral load, inflammatory markers and disease severity in HTLV-1 associated myelopathy/tropical spastic paraparesis (HAM/TSP). Retrovirology 6: 19.
17. Sakaguchi S, Yamaguchi T, Nomura T, Ono M (2008) Regulatory T cells and immune tolerance. Cell 133: 775–787.
18. Hattori T, Uchiyama T, Toibana T, Takatsuki K, Uchino H (1981) Surface phenotype of Japanese adult T-cell leukemia cells characterized by monoclonal antibodies. Blood 58: 645–647.
19. Uchiyama T, Hori T, Tsudo M, Wano Y, Umadome H, et al. (1985) Interleukin-2 receptor (Tac antigen) expressed on adult T cell leukemia cells. J Clin Invest 76: 446–453.
20. Karube K, Ohshima K, Tsuchiya T, Yamaguchi T, Kawano R, et al. (2004) Expression of FoxP3, a key molecule in CD4CD25 regulatory T cells, in adult T-cell leukaemia/lymphoma cells. Br J Haematol 126: 81–84.
21. Toulza F, Nosaka K, Takiguchi M, Pagliuca T, Mitsuya H, et al. (2009) FoxP3+ regulatory T cells are distinct from leukemia cells in HTLV-1-associated adult T-cell leukemia. Int J Cancer 125: 2375–2382.
22. Fontenot JD, Gavin MA, Rudensky AY (2003) Foxp3 programs the development and function of CD4+CD25+ regulatory T cells. Nat Immunol 4: 330–336.
23. Hori S, Nomura T, Sakaguchi S (2003) Control of regulatory T cell development by the transcription factor Foxp3. Science 299: 1057–1061.
24. Khattri R, Cox T, Yasayko SA, Ramsdell F (2003) An essential role for Scurfin in CD4+CD25+ T regulatory cells. Nat Immunol 4: 337–342.
25. Yasunaga J, Sakai T, Nosaka K, Etoh K, Tamiya S, et al. (2001) Impaired production of naive T lymphocytes in human T-cell leukemia virus type I-infected individuals: its implications in the immunodeficient state. Blood 97: 3177–3183.
26. Toulza F, Heaps A, Tanaka Y, Taylor GP, Bangham CR (2008) High frequency of CD4+FoxP3+ cells in HTLV-1 infection: inverse correlation with HTLV-1-specific CTL response. Blood 111: 5047–5053.
27. Richardson JH, Edwards AJ, Cruickshank JK, Rudge P, Dalgleish AG (1990) In vivo cellular tropism of human T-cell leukemia virus type 1. J Virol 64: 5682–5687.
28. Sugimoto M, Nakashima H, Watanabe S, Uyama E, Tanaka F, et al. (1987) T-lymphocyte alveolitis in HTLV-I-associated myelopathy. Lancet 2: 1220.
29. Bittencourt AL, de Oliveira Mde F (2010) Cutaneous manifestations associated with HTLV-1 infection. Int J Dermatol 49: 1099–1110.
30. Fontenot JD, Rasmussen JP, Gavin MA, Rudensky AY (2005) A function for interleukin 2 in Foxp3-expressing regulatory T cells. Nat Immunol 6: 1142–1151.
31. Sakaguchi S (2005) Naturally arising Foxp3-expressing CD25+CD4+ regulatory T cells in immunological tolerance to self and non-self. Nat Immunol 6: 345–352.
32. Lehmann J, Huehn J, de la Rosa M, Maszyna F, Kretschmer U, et al. (2002) Expression of the integrin alpha Ebeta 7 identifies unique subsets of CD25+ as well as CD25- regulatory T cells. Proc Natl Acad Sci U S A 99: 13031–13036.
33. Sather BD, Treuting P, Perdue N, Miazgowicz M, Fontenot JD, et al. (2007) Altering the distribution of Foxp3(+) regulatory T cells results in tissue-specific inflammatory disease. J Exp Med 204: 1335–1347.

34. Tone Y, Furuuchi K, Kojima Y, Tykocinski ML, Greene MI, et al. (2008) Smad3 and NFAT cooperate to induce Foxp3 expression through its enhancer. Nat Immunol 9: 194–202.
35. Wu Y, Borde M, Heissmeyer V, Feuerer M, Lapan AD, et al. (2006) FOXP3 controls regulatory T cell function through cooperation with NFAT. Cell 126: 375–387.
36. Ono M, Yaguchi H, Ohkura N, Kitabayashi I, Nagamura Y, et al. (2007) Foxp3 controls regulatory T-cell function by interacting with AML1/Runx1. Nature 446: 685–689.
37. Chae WJ, Henegariu O, Lee SK, Bothwell AL (2006) The mutant leucine-zipper domain impairs both dimerization and suppressive function of Foxp3 in T cells. Proc Natl Acad Sci U S A 103: 9631–9636.
38. Walker MR, Kasprowicz DJ, Gersuk VH, Benard A, Van Landeghen M, et al. (2003) Induction of FoxP3 and acquisition of T regulatory activity by stimulated human CD4+CD25- T cells. J Clin Invest 112: 1437–1443.
39. Wing K, Onishi Y, Prieto-Martin P, Yamaguchi T, Miyara M, et al. (2008) CTLA-4 control over Foxp3+ regulatory T cell function. Science 322: 271–275.
40. Wattel E, Vartanian JP, Pannetier C, Wain-Hobson S (1995) Clonal expansion of human T-cell leukemia virus type I-infected cells in asymptomatic and symptomatic carriers without malignancy. J Virol 69: 2863–2868.
41. Etoh K, Tamiya S, Yamaguchi K, Okayama A, Tsubouchi H, et al. (1997) Persistent clonal proliferation of human T-lymphotropic virus type I-infected cells in vivo. Cancer Res 57: 4862–4867.
42. Manel N, Kim FJ, Kinet S, Taylor N, Sitbon M, et al. (2003) The ubiquitous glucose transporter GLUT-1 is a receptor for HTLV. Cell 115: 449–459.
43. Jones KS, Petrow-Sadowski C, Bertolette DC, Huang Y, Ruscetti FW (2005) Heparan sulfate proteoglycans mediate attachment and entry of human T-cell leukemia virus type 1 virions into CD4+ T cells. J Virol 79: 12692–12702.
44. Lambert S, Bouttier M, Vassy R, Seigneuret M, Petrow-Sadowski C, et al. (2009) HTLV-1 uses HSPG and neuropilin-1 for entry by molecular mimicry of VEGF165. Blood 113: 5176–5185.
45. Koyanagi Y, Itoyama Y, Nakamura N, Takamatsu K, Kira J, et al. (1993) In vivo infection of human T-cell leukemia virus type I in non-T cells. Virology 196: 25–33.
46. Jones KS, Petrow-Sadowski C, Huang YK, Bertolette DC, Ruscetti FW (2008) Cell-free HTLV-1 infects dendritic cells leading to transmission and transformation of CD4(+) T cells. Nat Med 14: 429–436.
47. Vukmanovic-Stejic M, Zhang Y, Cook JE, Fletcher JM, McQuaid A, et al. (2006) Human CD4+ CD25hi Foxp3+ regulatory T cells are derived by rapid turnover of memory populations in vivo. J Clin Invest 116: 2423–2433.
48. Yamano Y, Takenouchi N, Li HC, Tomaru U, Yao K, et al. (2005) Virus-induced dysfunction of CD4+CD25+ T cells in patients with HTLV-I-associated neuroimmunological disease. J Clin Invest 115: 1361–1368.
49. Shimauchi T, Kabashima K, Tokura Y (2008) Adult T-cell leukemia/lymphoma cells from blood and skin tumors express cytotoxic T lymphocyte-associated antigen-4 and Foxp3 but lack suppressor activity toward autologous CD8+ T cells. Cancer Sci 99: 98–106.
50. Nerenberg M, Hinrichs SH, Reynolds RK, Khoury G, Jay G (1987) The tat gene of human T-lymphotropic virus type 1 induces mesenchymal tumors in transgenic mice. Science 237: 1324–1329.
51. Grossman WJ, Kimata JT, Wong FH, Zutter M, Ley TJ, et al. (1995) Development of leukemia in mice transgenic for the tax gene of human T-cell leukemia virus type I. Proc Natl Acad Sci U S A 92: 1057–1061.
52. Hasegawa H, Sawa H, Lewis MJ, Orba Y, Sheehy N, et al. (2006) Thymus-derived leukemia-lymphoma in mice transgenic for the Tax gene of human T-lymphotropic virus type I. Nat Med 12: 466–472.
53. von Boehmer H, Hafen K (1993) The life span of naive alpha/beta T cells in secondary lymphoid organs. J Exp Med 177: 891–896.
54. Asano T, Tomooka S, Serushago BA, Himeno K, Nomoto K (1988) A new T cell subset expressing B220 and CD4 in lpr mice: defects in the response to mitogens and in the production of IL-2. Clin Exp Immunol 74: 36–40.
55. Ishimoto Y, Tomiyama-Miyaji C, Watanabe H, Yokoyama H, Ebe K, et al. (2004) Age-dependent variation in the proportion and number of intestinal lymphocyte subsets, especially natural killer T cells, double-positive CD4+ CD8+ cells and B220+ T cells, in mice. Immunology 113: 371–377.
56. Hanon E, Hall S, Taylor GP, Saito M, Davis R, et al. (2000) Abundant tax protein expression in CD4+ T cells infected with human T-cell lymphotropic virus type I (HTLV-I) is prevented by cytotoxic T lymphocytes. Blood 95: 1386–1392.

研究成果の刊行に関する一覧表

研究分担者： 京都大学医学研究科附属ゲノム医学センター
松田　文彦

雑誌

発表者氏名	論文タイトル名	発表誌名	巻号	ページ	出版年
Nalpas, B., Laviall e-Meziani, R., Plan coulaine, S., Jouan guy, E., Nalpas, A., Munteanu, M., Charlotte, F., Ranq ue, B., Patin, E., Heath, S., Fontain e, H., Vallet-Pichar d, A., Pontoire, D., Bourlière, M., Casa nova, J. L., Lathro p, M., Bréchot, C., Poynard, T., Matsu da, F., Pol, S. and Abel, L.	Interferon-γ recept or 2 gene variant s are associated with liver fibrosis in patients with c hronic hepatitis C infection	Gut	59	1120-1126	2010
Hirosawa, K., Kaw aguchi, T., Matsud a, F. and Yamada, R.	Estimation of P-v alue of MAX test with double tria ngle diagram for 2 x 3 SNP case-control tables.	Genet. Epid emiol.	34	543-551	2010
Ohmura, K., Terao, C., Maruya, E., Ka tayama, M., Matob a, K., Shimada, K., Murasawa, A., Honjo, S., Takasug i, K., Tohma, S., Matsuo, K., Tajim a, K., Yukawa, N., Kawabata, D., Noji ma, T., Fujii, T., Yamada, R., Saji, H., Matsuda, F. an d Mimori, T.	Anti-citrullinated peptide antibody-negative RA is a genetically distinc t subset: a definit ive study using o nly bone-erosiveA CPA-negative rhe umatoid arthritis.	Rheumatolo gy	49	2298-2304	2010
Murakami, Y., Toy oda, H., Tanaka, M., Kuroda, M., H arada, Y., Matsuda, F., Tajima, A., K osaka, N., Ochiya, T. and Shimotohn o, K.	The Progression of Liver Fibrosis Is Related with Overexpression of the miR-199 and 200 Families.	PLoS One	6	e16081	2011

Interferon γ receptor 2 gene variants are associated with liver fibrosis in patients with chronic hepatitis C infection

Bertrand Nalpas,[1] Roubila Lavialle-Meziani,[2] Sabine Plancoulaine,[3,4] Emmanuelle Jouanguy,[3,5] Antoine Nalpas,[1] Mona Munteanu,[6] Frederic Charlotte,[6] Brigitte Ranque,[3,4] Etienne Patin,[3,4] Simon Heath,[2] Hélène Fontaine,[1,4] Anaïs Vallet-Pichard,[1,4] Dominique Pontoire,[7] Marc Bourlière,[8] Jean-Laurent Casanova,[3,4,9,10] Mark Lathrop,[2] Christian Bréchot,[11] Thierry Poynard,[6] Fumihiko Matsuda,[2,12] Stanislas Pol,[1,4] Laurent Abel[3,4,9]

► Supplementary tables are published online only. To view these files please visit the journal online (http://gut.bmj.com).

For numbered affiliations see end of article.

Correspondence to
Dr Laurent Abel, Laboratoire de Génétique Humaine des Maladies Infectieuses, Université Paris Descartes-INSERM U550, Faculté de Médecine Necker, 156 rue de Vaugirard, 75015 Paris, France;
laurent.abel@inserm.fr

Accepted 19 March 2010
Published Online First 29 June 2010

ABSTRACT

Background Only a minority of patients with chronic hepatitis C virus (HCV) infection develops severe liver fibrosis, a process that may be controlled by human genetic factors.

Objective To investigate the role of 384 single nucleotide polymorphisms (SNPs) located in 36 candidate genes related to the fibrogenesis/fibrolysis process.

Methods Patients with chronic HCV infection were gathered from two French cohorts (prospectively and retrospectively). The overall sample consisted of 393 HCV-infected subjects without known risk factors for fibrosis progression, including 134 patients with severe liver fibrosis and 259 without severe fibrosis.

Results Only two SNPs in strong linkage disequilibrium (LD) in the interferon γ receptor 2 gene (*IFNGR2*) were significantly associated with liver fibrosis in both the prospective and the retrospective samples. The strongest association ($p=8\times10^{-5}$) was observed with the G/A SNP rs9976971 with an OR of severe fibrosis for AA versus AG or GG subjects at 2.95 (95% CI 1.70 to 5.11). This effect was higher ($p=9\times10^{-7}$) when taking into account the time of follow-up, and the hazard ratio of progression towards severe fibrosis for AA patients was 2.62 (1.76 to 3.91). Refined sequencing and analysis of the *IFNGR2* region identified two additional variants in strong LD with rs9976971. No haplotypes derived from this cluster of four variants provided stronger evidence for association than rs9976971 alone.

Conclusions This identification of a cluster of four *IFNGR2* variants strongly associated with fibrosis progression in chronic HCV infection underlines the role of IFNγ in the development of liver fibrosis that may pave the way for new treatments.

Significance of this study

What is already known about this subject?

- Only a minority of patients with chronic HCV infection develops severe liver fibrosis.
- Viral and non-genetic host factors cannot account for the variability in the rate of progression towards liver fibrosis in patients with chronic HCV infection.
- There is accumulating evidence for the role of host genetic factors in the development of liver fibrosis, although these factors are as yet largely elusive.

What are the new findings?

- We investigated the role of 384 single nucleotide polymorphisms (SNPs) located in 36 candidate genes related to the fibrogenesis/fibrolysis process.
- We identified a single cluster of variants in the interferon γ receptor 2 gene (*IFNGR2*) strongly associated with progression to severe fibrosis.
- This association was replicated in an independent population sample, and was stronger when taking into account the time of follow-up from contamination to liver biopsy with a hazard ratio of developing severe fibrosis estimated as 2.62 (1.76 to 3.91) for the subjects homozygous for the predisposing allele.

How might it impact on clinical practice in the foreseeable future?

- As IFNγ is an anti-fibrogenic cytokine available for clinical purposes, our study may open new therapeutic avenues for the prevention of cirrhosis in HCV-infected patients.

INTRODUCTION

Hepatitis C virus (HCV) infection is a major public health concern world wide with an estimated 170 million people infected.[1 2] The natural history of patients with HCV chronic infection is characterised by a highly variable disease progression.[1–5] Most subjects never develop cirrhosis during their lifetime while the remaining patients are considered 'rapid fibrosers' and may develop severe fibrosis in <20 years.[1 5–7] While viral factors such as HCV genotypes or viral load do not seem to influence progression, several host factors such as gender (male), age at infection (>40 years old), alcohol consumption (>50 g/day), obesity and its related metabolic disorders, co-infections (in particular by HIV) are associated with the development of fibrosis.[4 5 8 9] However, these factors can account for only a minority of the variability in the rate of

progression, and a number of studies have investigated the role of genetic host factors.[5 10] Most of these studies have tested a single or a few candidate genes, and have not produced conclusive results as they were not clearly replicated.[10 11] A recent study investigated a large number (>24 000) of putative functional single nucleotide polymorphisms (SNPs) and identified two variants associated with severe fibrosis.[12] In a subsequent study which used the same SNPs and focused on Caucasian patients with well-characterised liver histology, a different panel of seven SNPs was found to predict the risk of developing cirrhosis, and this panel needs to be validated in prospective studies.[13]

Liver fibrosis is the consequence of a generalised wound-healing response of hepatic tissue against repeated injury, which results in the formation of scar tissue instead of normal parenchyma.[14] This process is characterised by an imbalance between matrix synthesis (ie, fibrogenesis) and matrix degradation (ie, fibrolysis), and leads to an accumulation of a large variety of matrix proteins, including collagens, proteoglycans and glycoproteins.[15 16] Activated hepatic stellate cells, portal fibroblasts and myofibroblasts of bone marrow origin are the major collagen-producing cells in the injured liver.[14] A number of molecules and regulatory pathways are involved in this complex process of fibrogenesis/fibrolysis.[14–16] Therefore, we hypothesised that variations in human genes involved in fibrogenesis/fibrolysis might account for interindividual variability in development of liver fibrosis among patients with chronic HCV infection. In this work we focused on the role of polymorphisms located in a panel of 36 genes (table 1) encoding either enzymes involved in extracellular matrix turnover (matrix metalloproteinases and their inhibitors) or some cytokines known to exhibit profibrogenic (transforming growth factor β (TGFβ) and related molecules) or anti-fibrogenic (interferon γ (IFNγ) and its receptors) activity. In addition to classic case–control analysis, in this study we analysed the influence of SNPs directly on the time of progression by restricting our sample to patients with a known presumed date of infection and without known risk factors of fibrosis progression such as chronic alcohol intake, associated infections or metabolic syndrome.

Table 1 List of the genes investigated in the association study

Gene name	Abbreviation
Alpha-2-macroglobulin	A2M
Angiotensinogen	AGT
Interferon gamma	IFNG
Interferon gamma receptor 1	IFNGR1
Interferon gamma receptor 2	IFNGR2
Keratin 8	KRT8
Latent transforming growth factor beta binding protein 1	LTBP1
Latent transforming growth factor beta binding protein 2	LTBP2
Latent transforming growth factor beta binding protein 3	LTBP3
Latent transforming growth factor beta binding protein 4	LTBP4
Matrix metalloproteinase 1	MMP1
Matrix metalloproteinase 2	MMP2
Matrix metalloproteinase 3	MMP3
Matrix metalloproteinase 7	MMP7
Matrix metalloproteinase 8	MMP8
Matrix metalloproteinase 9	MMP9
Matrix metalloproteinase 10	MMP10
Matrix metalloproteinase 11	MMP11
Matrix metalloproteinase 12	MMP12
Matrix metalloproteinase 13	MMP13
Matrix metalloproteinase 14	MMP14
Matrix metalloproteinase 15	MMP15
Matrix metalloproteinase 16	MMP16
Matrix metalloproteinase 17	MMP17
Matrix metalloproteinase 24	MMP24
Matrix metalloproteinase 25	MMP25
Transforming growth factor beta 1	TGFB1
Transforming growth factor beta 2	TGFB2
Transforming growth factor beta 3	TGFB3
Transforming growth factor beta receptor I	TGFBR1
Transforming growth factor beta receptor II	TGFBR2
Transforming growth factor beta receptor III	TGFBR3
Tissue inhibitor of metalloproteinase 1	TIMP1
Tissue inhibitor of metalloproteinase 2	TIMP2
Tissue inhibitor of metalloproteinase 3	TIMP3
Tissue inhibitor of metalloproteinase 4	TIMP4

PATIENTS AND METHODS

Patients

We recruited adult Caucasian patients (>18 years of age) with chronic HCV infection defined as the presence of circulating HCV RNA tested by reverse transcriptase PCR. The patients were gathered in two steps. First, we conducted a prospective enrolment of patients from the hepatology units of Necker Hospital in Paris and St Joseph Hospital in Marseille (sample A). The criteria for the inclusion of patients were (*a*) an available liver biopsy before any treatment; (*b*) a known presumed date of HCV acquisition (date of the first exposure to blood products, or of beginning of intravenous drug (IVD) use); (*c*) a low alcohol consumption (less than three or less than two standard drinks a day for men or women, respectively); (*d*) absence of co-infection with HIV or hepatitis B virus; (*e*) absence of any coexisting chronic liver disease or hepatocellular carcinoma. Clinical risk factors, history of HCV acquisition and of alcohol consumption (assessed using time-line follow-back interview) were recorded through face-to-face interviews conducted by doctors trained in addiction problems. In a second step, we gathered additional patients from an existing cohort from the hepatology unit of Pitié-Salpêtrière Hospital in Paris (sample B). The inclusion criteria were the same as for sample A except that the presumed date of infection was not known for all patients. The study was approved by the appropriate institutional review boards, and written informed consent was obtained from all patients.

Most of the enrolled patients had been followed up for a number of years in the corresponding clinics and had had a liver biopsy at the time of their first evaluation. The stage of fibrosis was assessed from liver biopsy samples using METAVIR units, and graded on a five-point scale from 0 to 4.[17] For this study, in order to optimise the phenotype definition, we excluded patients with grade 2, and retained only patients with grades 0 or 1 (F0–1 patients) referred to as having no fibrosis, and patients with grades 3 or 4 (F3–4) referred to as having severe fibrosis. For patients who had had several biopsies, we used either the first biopsy specimen showing severe fibrosis (F3–4 patients) or the last biopsy showing no fibrosis without any treatment (for F0–1 patients). The duration of infection was estimated from the presumed year of HCV acquisition (eg, first exposure to blood transfusion, or to IVD use) to the year of the relevant biopsy.

Genotyping and sequencing methods

In this study we focused on the role of polymorphisms located in a panel of genes encoding either enzymes involved in

extracellular matrix turnover (matrix metalloproteinases and their inhibitors) or cytokines that are believed to have a profibrogenic (TGFβ and related molecules) or an anti-fibrogenic (IFNγ and its receptors) activity. A total of 36 genes were selected and are shown in table 1. A selection of SNPs within each gene, totalling 384 SNPs (list in online supplementary table 1), was made using data from the first public release of HapMapII. For each gene, all HapMap SNPs in the region including the gene and the 10 kb flanking regions were initially considered. SNPs with minor allele frequency <5% or with low predicted quality for genotyping (calculated by Illumina) were filtered out, and pairwise linkage disequilibrium (LD) was estimated (from the HapMap data) between all pairs of remaining SNPs within each gene. The 384 SNP panel was then selected such that no two SNPs in the same gene had an estimated $r^2 \geq 0.8$ or were <60 bp apart.

All DNA samples were extracted from whole blood, and subjected to rigorous quality control to check for fragmentation and amplification. All SNPs were genotyped on an ultra-high throughput Illumina platform. This platform uses the GoldenGate assay followed by a bead-based technology to resolve individual SNP genotypes.[18] Discovery of SNPs within an *IFNGR2* region of ~12.3 kb from 33 689 894 to 33 702 179 bps on chromosome 21 was performed by exhaustive sequencing (figure 1). The sample consisted of 32 French Caucasian subjects (men and women with no disease history) from the Epidemiological study on the Genetics and Environment of Asthma.[19] The sample size of 32 allowed us to detect SNPs with a minor allele frequency of at least 5% with a probability of 96%. Sequencing reactions were performed with the Dye Terminator method using an ABI PRISM 3730 DNA Analyser (Applied Biosystems, Foster City, California, USA). Sequence alignment and SNP discovery were performed with Genalys software, developed by the Centre National de Génotypage (CNG).[20]

Statistical methods

Association between severe fibrosis and the panel of SNPs was first tested in sample A by a case–control analysis using the genotypic test statistic (two degrees of freedom): the cases are HCV-infected patients with severe fibrosis and the controls are infected patients without severe fibrosis. When a type I error of 0.02 was used, our initial sample A had a power of 80% for detecting a polymorphism with an additive effect, providing an odds ratio (OR) for heterozygosity of two and having a frequency >0.09. For SNPs showing association at p<0.02, we then tested association by a survival analysis approach using a Cox model: we considered as starting points the estimated ages at infection, and as end points either the first biopsy showing severe fibrosis (failure time) or the last biopsy showing absence of severe fibrosis in the absence of any treatment (censored time). For all these analyses, we determined the genetic model (dominant/additive/recessive) providing the best fit to the data. SNPs showing the most interesting results (p<0.02 in the case–control study and p<0.05 in the survival analysis) were then tested for replication in sample B.

We tested for heterogeneity of the association results according to different criteria, such as gender, mode of infection (blood transfusion/IVD use/others), viral genotypes (one and four vs others), age at infection (≤20 years vs >20 years). Under the hypothesis of homogeneity of association, twice the difference between the likelihood of the whole sample and the summed likelihoods of the subsamples (eg, the two subsamples of men and women) is asymptotically distributed as a χ^2 with one degree of freedom. All statistical analyses were performed using different procedures (FREQ, LOGISTIC, PHREG) implemented in SAS software version 8.2 (SAS Institute). Pairwise LD between SNPs was assessed by determining the r^2 coefficient using the Haploview software.[21] Haplotype analysis was conducted using the THESIAS software (http://www.genecanvas.org, accessed 5 May 2010).[22]

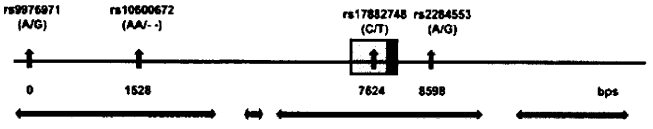

Figure 1 Schematic representation of the chromosome 21 region ranging from 33 689 800 to 33 702 200 bps, and including the 5′ region, exon 1 and part of intron 1 of *IFNGR2*. Exon 1 ranges from 33 697 072 to 33 697 792 bp with an untranslated and a translated part shown as a hatched and a solid box, respectively. Horizontal arrows indicate the regions covered by direct sequencing. Three segments could not be sequenced for technical reasons (33 694 486–33 696 000, 33 696 161–33 696 390 and 33 699 114–33 700 075 bp). The four single nucleotide polymorphisms associated with severe fibrosis are indicated by vertical arrows with distance in base pairs provided from the position of rs9976971, which is located at 33 689 967 bp.

RESULTS

Description of the two samples

Samples A and samples B consisted of a total of 267 (103 F3–4 patients with severe fibrosis and 164 F0–1 patients without severe fibrosis), and 126 (31 F3–4 and 95 F0–1 patients) patients with chronic HCV infection, respectively. The main features of the overall sample including 393 patients are shown in table 2. There was an overall excess of women (58.5% vs 41.5%, $p=8\times10^{-4}$), which might be explained, in part, by the inclusion criterion of low alcoholic consumption, but there was no significant difference (p=0.24) in the distribution of gender according to fibrosis status. In the 364 patients with reliable HCV acquisition data, the overall distribution of modes of infection was different (p=0.0004) according to the fibrosis status. The proportion of patients infected by blood transfusion was higher in patients with severe fibrosis (57.5%) than in F0–1 patients (41.3%), while the reverse was observed for IVD users (43% in F0–1 patients vs 22% in F3–4 patients). F3–4 patients were significantly older (p=0.004) at infection (mean 29.9 years, range 0.1–73.2 years) than F0–1 patients (25.6 years, 0.1–70.8 years), and had a longer ($p=10^{-4}$) duration of HCV infection at the time of biopsy (22.8 years, 0.7–49.6 years vs 18.9 years, 0.2–49.6 years). Finally, the distribution of viral genotypes combined as usual in three main groups according to their sensitivity to anti-viral treatment[23] was not significantly different between F0–1 and F3–4 patients.

Four variants are associated with fibrosis in the first sample

Of the 384 SNPs, 16 SNPs could not be genotyped (supplementary table 1), and we excluded an additional five SNPs because either they showed deviations (p<0.005) from Hardy–Weinberg equilibrium (three SNPs) or they had a minor allele frequency <0.02 (two SNPs). The 363 remaining SNPs all showed a genotyping success >96%, and were used for association analysis. Association between severe fibrosis and the panel of 363 SNPs was first tested in sample A by a classic case–control analysis where cases were the HCV-infected patients with severe fibrosis and controls were the infected patients without severe fibrosis (supplementary table 1). A total of nine

Table 2 Main features of the HCV chronically infected patients in the whole sample

	METAVIR fibrosis score		
	F0–1	F3–4	Total
Number of patients	259	134	393
Sex ratio (male/female)	0.65	0.84	0.71
Mode of infection			
Blood transfusion	98	73	171
IVD	102	28	130
Others	37	26	63
Unknown	22	7	29
Age at contamination (years)*	25.6 (12.1)†	29.9 (14.0)	27.1 (12.9)
Duration of infection (years)*	18.9 (8.2)	22.8 (9.6)	20.3 (8.9)
Viral genotypes			
1A, 1B, 4	157	96	253
2, 5	27	8	35
3	49	19	68
Unknown	26	11	37

*Data for the 364 patients with known presumed dates of acquisition.
†mean (SD).
IVD, intravenous drug.

SNPs, including two in *IFNGR2* and three in *MMP16*, provided evidence for association with a p value <0.02, and were investigated further. Of these nine SNPs, four significantly influenced ($p<0.05$) the rate of progression towards severe fibrosis when performing a survival analysis (table 3 and supplementary table 2). The effects of the two *IFNGR2* SNPs, rs9976971 and rs2284553, which already yielded the lowest p values in the case–control study ($p=3\times10^{-4}$ and $p=8\times10^{-4}$, respectively), were even more significant ($p=2\times10^{-5}$ and $p=8\times10^{-5}$, respectively) using the survival analysis. Conversely, the effects of the two other SNPs (one in *MMP16*, and one in *TGFBR2*) were slightly lower when accounting for time of progression. For both rs9976971 and rs2284553 (which are G/A SNPs), the risk allele was the minor allele A and the best fitting genetic model was recessive—that is, subjects who were AA homozygous were predisposed to severe fibrosis as compared with AG and GG subjects. These two SNPs were in strong LD ($r^2=0.79$), and multivariate analysis confirmed that the results observed with rs9976971 and rs2284553 reflect a single signal.

Two *IFNGR2* variants show evidence for replication in the second sample

The four SNPs providing evidence for association both in case–control (at $p<0.02$) and survival (at $p<0.05$) were tested in sample B (table 3). Only the two *IFNGR2* SNPs showed evidence for replication with the same risk allele. As in sample A, the survival analysis was more powerful than the case–control approach, leading to a significant effect in sample B for rs9976971 (p=0.011). A similar trend, although not significant (p=0.13), was observed for rs2284553. When samples A and B were combined (table 4), the overall effect of rs9976971 in the case–control design was highly significant ($p=8\times10^{-5}$), and the OR (95% CI) of presenting severe fibrosis for AA subjects as compared with AG or GG subjects was 2.95 (1.70 to 5.11). This effect was much stronger ($p=9\times10^{-7}$) in the survival analysis design, and the HR (95% CI) of progressing towards severe fibrosis for AA subjects as compared with AG or GG subjects was 2.62 (1.76 to 3.91) (figure 2).

Consistent with this result taking into account the duration of infection, we observed that the effect of rs9976971 in the classical case–control design was much stronger (OR=4.46 (2.28 to 8.72)) in the 57 F3–4 patients with rapid progression (≤20 years of infection) than in the 69 F3–4 patients with slow progression (>20 years of infection, OR=2.10 (1.04 to 4.25)). Even if we considered the fact that these results were obtained in a one-step strategy (without the use of a replication sample), and that we applied the classical and stringent Bonferroni correction for multiple testing (assuming we have tested the 363 SNPs in the whole sample), the corrected p values for rs9976971 remained significant and equal to 0.029 and 0.0003 in the case–control and the survival analysis, respectively. These results indicate that one SNP in *IFNGR2*, either rs9976971 or another variant in strong LD with it, strongly influences the rate of progression towards severe fibrosis in patients chronically infected by HCV.

Search for other polymorphisms in linkage disequilibrium with the two *IFNGR2* variants

Next, we searched for other variants in strong LD with rs9976971 along three lines. First, we looked for long range LD (from 33 380 000 to 34 000 000 bp) using the European population of the HapMap database, NCBI build 36 (http://www.hapmap.org/, accessed 5 May 2010). Substantial LD (r^2 ranging from 0.3 to 0.48) with rs9976971 was observed with three clusters of SNPs. We genotyped one tag-SNP within each cluster (rs2834208, rs13047599, and rs7279549), and no association with severe fibrosis ($p>0.2$) was observed with any of these tag-SNPs. No other SNPs showed $r^2>0.3$ within this interval, and, in particular, all SNPs between 33 524 000 and 33 655 000 bp where the genes *IFNAR1* and *IFNAR2* encoding interferon α/β receptors are located, provided $r^2<0.11$ with rs9976971. Second, we explored the SeattleSNPs variation discovery resource database as it contained results for *IFNGR2*

Table 3 Results in both samples for the four single nucleotide polymorphisms (SNPs) providing the strongest evidence for association with severe fibrosis in sample A (ie, $p<0.02$ in case–control study and $p<0.05$ in the survival analysis). The full distribution of genotypes for these four SNPs is shown in online supplementary table 2

				Sample A				Sample B			
				Case/control (n=103/164)		Survival analysis (n=267)		Case/control (n=31/95)		Survival analysis (n=97)	
Marker	Gene	Risk allele (frequency)	Model*	OR (95% CI)†	p	HR (95% CI)‡	p	OR (95% CI)	p	HR (95% CI)	p
rs2284553	IFNGR2	A (0.41§)	rec	3.10 (1.57 to 6.13)	8×10^{-4}	2.41 (1.54 to 3.79)	8×10^{-5}	1.02 (0.26 to 4.05)	-¶	3.01 (0.66 to 13.7)	0.13
rs9976971	IFNGR2	A (0.44)	rec	3.22 (1.68 to 6.18)	3×10^{-4}	2.54 (1.64 to 3.93)	2×10^{-5}	2.04 (0.68 to 6.17)	0.19	3.56 (1.26 to 10.1)	0.011
rs2664357	MMP16	C (0.27)	add	1.86 (1.24 to 2.79)	0.002	1.47 (1.12 to 1.93)	0.006	0.62 (0.32 to 1.21)	0.16	0.81 (0.40 to 1.65)	–
rs9831477	TGFBR2	T (0.58)	dom	2.93 (1.35 to 6.38)	0.005	2.27 (1.14 to 4.50)	0.016	1.58 (0.49 to 5.08)	–	0.97 (0.32 to 2.91)	–

*Genetic model (recessive (rec), additive (add), or dominant (dom)) for the risk allele.
†OR (with 95% CI) under the corresponding genetic model.
‡HR (with 95% CI) under the corresponding genetic model estimated by Cox model analysis.
§frequency estimated in sample A.
¶$p > 0.2$.

Table 4 Results in the whole sample for the four *IFNGR2* variants providing the strongest evidence for association

Marker (type)	Position	Genotypes	No fibrosis F0–1, n (%)	Fibrosis F3–4, n (%)	Case/control study		Survival analysis	
					OR (95% CI)	p	HR (95% CI)	p
rs9976971 (G/A SNP)	33689967* 5′ region†	GG and AG	231 (89.2)	98 (73.7)	1		1	
		AA	28 (10.8)	35 (26.3)	2.95 (1.70 to 5.11)	8×10^{-5}	2.62 (1.76 to 3.91)	9×10^{-7}
		Total	259	133				
rs10600672 (AA/– ins/del)	33691495 5′ region	–/– and AA/–	228 (88.4)	98 (73.1)	1		1	
		AA/AA	30 (11.6)	36 (26.9)	2.79 (1.63 to 4.79)	10^{-4}	2.47 (1.66 to 3.66)	4×10^{-6}
		Total	258	134				
rs17882748 (T/C SNP)	33697591 Exon 1, 5′UTR	TT and CT	216 (83.7)	92 (68.7)	1		1	
		CC	42 (16.3)	42 (31.3)	2.35 (1.43 to 3.84)	6×10^{-4}	2.05 (1.40 to 3.01)	2×10^{-4}
		Total	258	134				
rs2284553 (G/A SNP)	33698565 Intron 1	GG and AG	233 (90.3)	105 (78.4)	1		1	
		AA	25 (9.7)	29 (21.6)	2.57 (1.44 to 4.61)	0.001	2.39 (1.57 to 3.66)	3×10^{-5}
		Total	258	134				

*Position in base pairs on chromosome 21.
†position relative to *IFNGR2* gene.

sequencing in 23 European subjects for a region of ~ 38 kb (33 695 200–33 733 200) (http://pga.gs.washington.edu/data/ifngr2/, accessed 5 May 2010). Finally, as rs9976971 is located in 5′ of *IFNGR2* (33 689 967), we also sequenced a sample of 32 French Caucasian subjects for a region of 12.3 kb from 33 689 894 to 33 702 179 (figure 1 and supplementary table 3). Based on these sequencing data from both the SeattleSNPs database and our own results, we identified two additional variants in strong LD with rs9976971 (table 4). One is the T/C SNP rs17882748 (r^2=0.83 with rs9976971) located in the untranslated region of exon 1, and the other is an AA insertion/deletion denoted as rs10600672 (r^2=0.98 with rs9976971) located in the 5′ region of the gene at position 33 691 495.

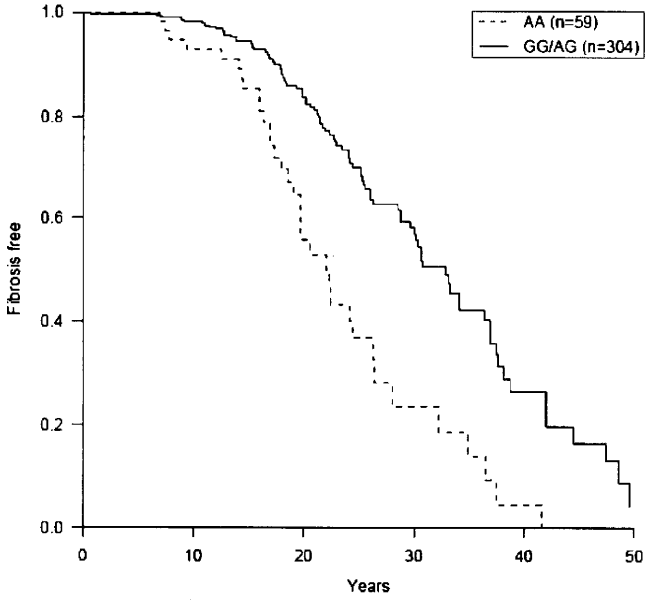

Figure 2 Effect of single nucleotide polymorphism rs9976971 on fibrosis progression. The figure shows the variation with time of the proportion of fibrosis-free patients according to genotypes at rs9976971. The time of follow-up was estimated from the presumed year of infection to the year of either the first biopsy showing severe fibrosis (F3–4 patients) or the last biopsy showing no fibrosis without any treatment (for F0–1 patients).

A cluster of four *IFNGR2* variants is strongly associated with liver fibrosis progression

Table 4 shows the results of both the case–control and the survival analysis with the four variants of interest over the combined samples A and B. Although all variants were strongly associated with development of severe fibrosis, the most significant results were observed with rs9976971 ($p=9\times10^{-7}$) and the AA ins/del ($p=4\times10^{-6}$) when using survival analysis. The AA insertion is in almost perfect LD with the A allele of rs9976971 (only three subjects had discordant genotypes) so that the HR of progressing towards severe fibrosis for AA/AA subjects as compared with AA/– or –/– subjects was 2.47 (1.66 to 3.66), and the curve of progression towards fibrosis with age according to this ins/del variant was extremely similar to that shown in figure 2 for rs9976971. We did not find any significant heterogeneity of these associations according to gender, mode of infection (blood transfusion/IVD use/others), viral genotypes (1 and 4 vs others), age at infection (≤20 years vs >20 years). We also conducted an analysis considering the different haplotypes that could be derived from these four variants using the method developed in the THESIAS program.[22] As expected by LD, two common haplotypes accounted for >90% of the estimated haplotypes (table 5). The common haplotype carrying the risk alleles at the four *IFNGR2* variants had a frequency of 0.338 and 0.447 in F0–1 and F3–4 patients, respectively. Under a recessive model (table 5), the effects of this at-risk haplotype (using a case–control or a survival analysis) were slightly lower than those estimated from rs9976971 or rs10600672 alone. As expected by the r^2 value at 0.98, the two variant haplotypes consisting of rs9976971 and rs10600672 provided results almost identical to the analysis of any of these variants alone (data not shown). However, none of the tested haplotypes consisting of three or four of these *IFNGR2* variants provided stronger evidence for association than rs9976971 or rs10600672 when considered alone.

DISCUSSION

In this study, we investigated whether the development of liver fibrosis in HCV chronically infected patients might be influenced by polymorphisms located in a panel of 36 genes involved in the fibrogenesis/fibrolysis process. To reduce the variability in assessing fibrosis stage by biopsy,[24] only F0–1 and F3–4 stages were included to define phenotypes. We found a single convincing signal of association in *IFNGR2*, which was the most

Table 5 Results of the analysis considering haplotypes derived from the cluster of the four *IFNGR2* variants providing the strongest evidence for association

Polymorphisms				Haplotype frequencies		Case–control study		Survival analysis	
rs9976971	rs10600672	rs17882748	rs2284553	No fibrosis	Fibrosis	OR (95% CI)	p	HR (95% CI)	p
G	–	T	G	0.570	0.466				
A	AA	C	A	0.338	0.447	2.70 (1.48 to 4.92)*	0.0011	2.32 (1.52 to 3.56)*	10^{-4}
G	–	T	A	0.049	0.034				
A	AA	T	A	0.035	0.034				
A	AA	C	G	0.004	0.004				
G	AA	C	A	0.004	0.004				

*Results obtained with a recessive model for the common haplotype A/AA/C/A consisting of the risk alleles of the four *IFNGR2* variants.

significant in our primary sample and was exactly replicated (same allele at risk and same genetic model) in our second sample. The evidence for association was even higher (by one order of magnitude) when using the information obtained by the time of progression, providing strong additional support for our findings. The *IFNGR2* signal results from a cluster of four variants in strong LD. These variants are quite common with a frequency in the HapMap Caucasian population of 0.41 for risk allele A of the most associated SNP rs9976971, and 26% AA homozygosity in our sample of F3–4 patients. Sequencing data obtained either from existing databases or from our present analysis excluded the role of any other SNPs located within a region of ~43.5 kb (33 689 894–33 733 200 bps) encompassing the *IFNGR2* gene. Analysis of the HapMap database also made quite unlikely the hypothesis that this signal could be due to another SNP in long-range LD with this cluster of four *IFNGR2* variants. Refined analysis showed that no haplotypes derived from this cluster of four variants provided stronger evidence for association than any of the four SNPs when analysed alone. From a statistical point of view, the strongest evidence was obtained with rs9976971 and the AA ins/del (rs10600672), which are in almost perfect LD. Nevertheless, the roles of rs2284553 (in intron 1) and rs17882748 (in untranslated region of exon 1) could not be ruled out.

Although several association studies have investigated the role of a small number of polymorphisms within the gene encoding IFNγ (*IFNG*) and progression to fibrosis in HCV infection, in particular a variant at position +874 which may influence IFNγ expression, no consistent and clearly replicated results have been reported.[10] A study also tested the role of variants within the interferon γ receptor 1 gene (*IFNGR1*), without any significant results.[25] In this context, it is interesting to note that two linkage studies conducted in Sudan[26] and Egypt[27] mapped a locus predisposing to development of severe liver fibrosis due to the parasite *Schistosoma mansoni* infection in a region including the *IFNGR1* gene. No precise variants underlying these linkage peaks have been reported yet. To our knowledge, no studies have yet investigated the influence of *IFNGR2* polymorphisms in HCV-related liver fibrosis. We cannot rule out the possibility that some *IFGNR2* variants were included in the study that tested the association with 24 823 putative functional SNPs.[12] However, it is unlikely that any of our four associated polymorphisms were included in that panel as they are not known to be functional.

IFNγ is usually considered to be an anti-fibrogenic cytokine. In an experimental model of liver fibrosis induced with carbon tetrachloride, IFNγ-deficient mice exhibited more pronounced hepatic fibrosis lesions than wild-type animals, and exogenous IFNγ administered to deficient animals reduced the level of fibrosis.[28] In human cells, IFNγ has been shown to inhibit activation, proliferation and collagen synthesis in cultures of activated hepatic stellate cells and hepatic myofibroblasts.[16 29] It is also interesting to note that IFNγ has been proposed as a treatment for idiopathic pulmonary fibrosis and was associated with reduced mortality in a meta-analysis.[30] Along the same lines, high levels of IFNγ production were associated with protection against periportal fibrosis in subjects infected with the parasites *S mansoni*[31] or *Schistosoma japonicum*.[32]

However, the role of IFNγ may be more complex, as suggested by a study performed on liver biopsy specimens from patients with chronic HCV infection, which showed that increased IFNγ expression was associated with portal inflammation and fibrosis stage.[33] This latter observation suggests that the proinflammatory effects of IFNγ may predominate over its anti-fibrogenic role in HCV liver fibrosis, although IFNγ expression might also be a consequence of the fibrosis process. For example, an impaired function of IFNγ receptors might lead to increased production of IFNγ, as seen in patients with complete IFNγ receptor deficiencies.[34]

In conclusion we have found that progression to severe liver fibrosis in HCV chronically infected patients of European origin is strongly associated with a cluster of four *IFNGR2* variants. Interestingly, between the two IFNγ receptors, IFNγR2 expression appears to be the deciding factor that controls the way in which target cells physiologically respond to IFNγ.[35 36] Functional studies are continuing in human liver cells to investigate the detailed biological mechanisms of this association and the potential effect of this cluster of variants on *IFNGR2* regulation. Prospective studies using large samples will also assess the predictive value of these polymorphisms with repeated validated non-invasive biomarkers.[37] IFNγ has already been found to be associated with clearance of HCV infection.[38 39] These results highlight the role of the IFNγ pathway in development of liver fibrosis that may pave the way for new treatments.

Author affiliations
[1]Unité d'Hépatologie, Institut National de la Santé et de la Recherche Médicale, U567, Hôpital Cochin, Paris, France
[2]Centre National de Génotypage, Evry, France
[3]Laboratory of Human Genetics of Infectious Diseases, Necker Branch, Institut National de la Santé et de la Recherche Médicale, U550, Necker Medical School, Paris, France
[4]Université Paris Descartes, Paris, France
[5]Center for the Study of Hepatitis C, The Rockefeller University, New York, USA
[6]Assistance Publique-Hôpitaux de Paris (AP-HP)/Université Pierre et Marie Curie (UPMC) Liver Center, Hôpital Pitié-Salpêtrière, Paris, France
[7]Banque de Cellules Cochin-APHP, Service de Biochimie et Génétique Moléculaire, Hôpital Cochin, Paris, France
[8]Department of Hepato-gastroenterology, Hôpital Saint Joseph, Marseille, France
[9]Laboratory of Human Genetics of Infectious Diseases, Rockefeller Branch, The Rockefeller University, New York, USA
[10]Pediatric Hematology and Immunology Unit, Necker Children's Hospital, Paris, France
[11]Institut National de la Santé et de la Recherche Médicale, U785, Villejuif, France
[12]Unit of Human Disease Genomics, Institut National de la Santé et de la Recherche Médicale, Kyoto University, Kyoto, Japan